Role of GD2 and its biosynthetic enzyme GD3 synthase in prostate cancer tumorigenesis

Aaqib M. Bhat[1,2,*], Bhopal C. Mohapatra[2,8,*,#], Haitao Luan[1], Insha Mushtaq[1,3], Sukanya Chakraborty[1,2], Samikshan Dutta[4], Matthew D. Storck[1], Jane L. Meza[5,8], Ming-Fong Lin[4], Leah M. Cook[3,8], Eva Corey[6], Colm Morrissey[6], Donald W. Coulter[7,9], M. Jordan Rowley[2,8], Kaustubh Datta[4,8], Vimla Band[2,8,#], Hamid Band[1,2,3,4,8,#]

[1]Eppley Institute for Research in Cancer and Allied Diseases, University of Nebraska Medical Center, Omaha, NE; [2]Department of Genetics, Cell Biology and Anatomy, College of Medicine, University of Nebraska Medical Center, Omaha, NE; [3]Departments of Pathology & Microbiology, College of Medicine, University of Nebraska Medical Center, Omaha, NE; [4]Department of Biochemistry and Molecular Biology, University of Nebraska Medical Center, Omaha, NE; [5]Department of Biostatistics, College of Public Health, University of Nebraska Medical Center, Omaha, NE; [6]Department of Urology, University of Washington, Seattle, WA; [7]Department of Pediatrics, University of Nebraska Medical Center, Omaha, NE; [8]Fred & Pamela Buffett Cancer Center, University of Nebraska Medical Center, Omaha, NE.

***Co-First Authors**

Running Title: GD2 in prostate cancer tumorigenesis

[#]**Corresponding authors:** Hamid Band, MD, PhD, Eppley Institute for Research in Cancer and Allied Disease, 986805 Nebraska Medical Center, Omaha, NE 68198-6805, USA; Email: hband@unmc.edu; Phone: 402-559-8572
Bhopal C. Mohapatra, PhD, Department of Genetics Cell Biology & Anatomy, University of Nebraska Medical Center, 985805 Nebraska Medical Center, Omaha, NE, 68198, USA. bmohapat@unmc.edu; Phone: 402-559-8542
Vimla Band, PhD, Department of Genetics Cell Biology & Anatomy, University of Nebraska Medical Center, 985805 Nebraska Medical Center, Omaha, NE, 68198, USA; Email: vband@unmc.edu; Phone: 402-559-8572

Conflict of interest disclosure statement: Dr. H. Band and Dr. V. Band received funding from Nimbus Therapeutics for an unrelated project.

Word count: Abstract -213, Manuscript – Main text-5453, Methods- 1616
Figures: 06; **Supplementary Figures**: 05 and 1 table

ABSTRACT

While better management of loco-regional prostate cancer (PC) has greatly improved survival, advanced PC remains a major cause of cancer deaths. Novel, targetable, pathways that contribute to tumorigenesis in advanced PC could open new therapeutic options. The di-ganglioside GD2 is a target of FDA-approved antibody therapies in neuroblastoma, but any role of GD2 in PC is little explored. Here, we show that GD2 is expressed on a small subpopulation of tumor cells in a subset of PC patients, especially in metastatic PC. Variable levels of cell surface GD2 expression are seen in most PC cell lines, and the expression is highly upregulated by experimental induction of lineage progression or enzalutamide resistance in CRPC cell models. GD2+ fraction is enriched upon growth of PC cells as tumorspheres and GD2+ fraction is enriched in tumorsphere growth. CRISPR-Cas9 knockout (KO) of the rate-limiting GD2 biosynthetic enzyme GD3 Synthase (GD3S) in GD2-high CRPC cell models led to marked impairment of their *in vitro* oncogenic traits, reduced cancer stem cell and epithelial-mesenchymal transition marker expression and growth as bone-implanted xenograft tumors. Our results support a potential role of GD3S and its product GD2 in promoting PC tumorigenesis, likely by its recently demonstrated role in maintaining cancer stem cells and suggest the potential for GD2 targeting in advanced PC.

INTRODUCTION:

Despite gains from early diagnoses, the successful use of androgen derivation therapy (ADT) and the introduction of androgen receptor (AR) signaling inhibitors (ARSIs) as targeted agents, prostate cancer (PC) remains a major killer of men and the low survival of patients with distant metastases remains a major challenge. A key transition towards less controllable and incurable metastatic disease is the emergence of castration-resistant PC (CRPC). This has prompted search for targetable pathways that are key to CRPC tumorigenesis. Pathways that can be targeted using existing agents with acceptable safety profiles in clinic are particularly attractive as their transition along the translational-clinical continuum can be expected to proceed swiftly in order to positively impact the course of advanced disease.

The cell-surface di-ganglioside GD2 is expressed on developing neuroectodermal cells and, at lower levels, in certain adult tissues like neurons and basal cells of the skin (1). Biochemically, GD2 is a b-series ganglioside generated from lactosyl-ceramide, which is serially converted to GM3, GD3 and GD2 by the actions of enzymes ST3GAL3 (GM3 synthase), ST8SIA1 (GD3 synthase; GD3S) and B4GALNT1 (GM2/GD2 synthase; GD2S), respectively, with GD3S considered rate-limiting (2) (**Fig. 1A**). GD2 is highly expressed on nearly all neuroblastomas, most melanomas and retinoblastomas, and many Ewing sarcomas; it is also overexpressed on some cases of small cell lung cancer, gliomas, osteosarcomas, and soft tissue sarcomas (3).

Functionally, GD2 has been implicated in oncogenic signaling leading to increased cell proliferation, migration, and invasion, and designated by the NCI as the top 12th among 75 tumor antigens (4). Extensive studies have led to the development of GD2-taregted antibodies for maintenance therapy of neuroblastoma patients (5,6), with clinical studies demonstrating the safety and efficacy of this approach (7). A humanized anti-GD2 monoclonal antibody with a higher

affinity for GD2 was recently approved for children and adults with relapsed or refractory high-risk neuroblastoma (8).

Validation of GD2 targeting as a therapeutic approach in neuroblastoma has prompted studies of other cancers for the role of GD2 and its potential targeting (3). Significant insights in this direction have come from studies of breast cancer. Unlike neuroblastoma and other tumors characterized previously, where a majority of tumor cells express GD2, human breast cancer cell lines and patient samples harbor a small $GD2^+$ fraction which selectively formed tumorspheres *in vitro* and tumors when implanted *in vivo*, and was enriched in triple-negative breast cancer (TNBC) subtype known to be more aggressive and metastasis-prone; the $GD2^+$ breast cancer cells were $CD44^{hi}/CD24^{lo}$, indicating that GD2 stained the previously-identified cancer stem cell (CSC) fraction, and GD3S knockdown reduced the CSC population and CSC-associated properties and abrogated tumor formation in vivo (9,10). Further, GD3S knockdown or inhibition of its expression by triptolide was found to inhibit the EMT and migratory/invasive behavior *in vitro* and abrogate metastasis *in vivo* in claudin-low (mesenchymal) breast cancer cell lines (11). Finally, Dinutuximab was found to inhibit experimental triple-negative breast tumor growth by targeting CSCs (12). Recently, O-acetyl-GD2 was also found to mark breast cancer CSCs (13). GD2 expression on breast cancer CSCs also allowed synergistic targeting by human γδ and $CD8^+$ T cells together with humanized anti-GD2 antibody hu14.18K322A (14). Further, GD2-CAR expressing T cells inhibited the orthotopic breast cancer xenograft growth and completely prevented lung metastasis by eliminating CSCs (15). GD2 expression also correlated with CSC markers and EMT in bladder cancer cells (16). GD3S and GD3 (17) as well as O-acetyl-GD2 (17) were found to drive glioblastoma CSCs and tumorigenicity, with sensitization of tumor cells to temozolomide *in vitro* and *in vivo* by anti-O-acetyl-GD2 antibody. Thus, GD2 and its rate-limiting

biosynthetic enzyme GD3S have emerged as key factors in promoting CSC behavior and as targets of CSC-directed therapeutic efforts (18,19). As CSCs are key to initiation and maintenance of tumors, and responsible for therapeutic resistance, and metastasis (20), targeting of GD2 in this tumor cell subpopulation represents a significant shift in thinking about the role of this ganglioside and the enzymatic machinery responsible for its expression in non-neuroblastoma tumors.

Progression to CRPC is associated with increased CSC features and EMT (21). However, few, mostly older, studies have explored the status of GD2 in PC. An early study of a small number of prostate hyperplasia, prostate cancer, and normal prostate tissue samples by thin layer chromatography found that GD2 levels were reduced during tumorigenesis (22). Another study detected more GD2 expression by chromatography in AR-negative PC cell lines (HH870, DU145 and PC-3) than in AR^+ cell lines (LNCaP clones FGC and FGC-10), and immunofluorescence analyses showed the expression of cell surface GD2 on PC3 but not a normal prostate epithelial cell line (23,24). A recent study found higher expression of a long non-coding RNA (lncRNA) MIR4435-2HG in PC cell lines (VCAP, LNCaP, DU145 and PC-3) compared to a normal prostate epithelial cell line and its knockdown reduced while ectopic overexpression increased the PC3 cell proliferation, migration and invasion in vitro and tumorigenesis *in vivo*; MIR4435-2HG was found to bind to GD3S mRNA and promote its expression, and GD3S knockdown (which by itself had no impact) was found to reduce the pro-tumorigenic effects of ectopic MIR4435-2HG overexpression (25). This study did not examine the ganglioside products of GD3S, and reported high GD3S expression in all 4 PC cell lines examined; the latter is not confirmed by our analysis of the mRNA expression of the same cell lines reported in a comprehensive epigenetics/transcriptomics study (26) and our analyses demonstrate little or no GD2 expression on some of these PC cell lines (See Results). Any functional role(s) of GD2 in PC remain unknown

and its targeting in PC has never been explored despite considerable progress on the role of GD2 in other cancers and its successful targeting in neuroblastoma.

Here, we carry out analyses of GD2 expression in prostate cancer patient tissues and their metastases as well as in cell line models of CRPC progression and use CRISPR-KO of GD3S in a human and murine CRPC cell line models to establish that GD2 expression is a feature of a small fraction of tumor cells enriched in tumorsphere growth in vitro, and that GD3S is required for tumorigenesis in CRPC.

MATERIALS AND METHODS:

Prostate cancer (PC) patient tissue microarrays and immunohistochemical analysis: Tissue microarrays (TMAs) composed of paired normal prostate and prostate cancer Gleason grades (3, 4 and 5; n = 320) and or of 45 cases of bone and visceral metastatic samples from Rapid Autopsy TMAs were obtained without any identifying patient information from the Prostate Cancer Biorepository Network (PCBN) repository under a materials transfer agreement. TMAs were stained for GD2 by immunohistochemistry (IHC) as described previously (27). Briefly, TMAs were deparaffinized in xylene, rehydrated in descending alcohols and heated in the antigen retrieval solution (vector, cat#H-3300) in a microwave to unmask the antigens. Endogenous peroxidase activity was blocked by incubation in 3% hydrogen peroxide for 20 min. The sections were rinse in phosphate buffered saline (PBS) and blocked in Protein-Block buffer (DakoCytomation #0909) for 15 min. The sections were then stained with anti-GD2 antibody (2 μg/ml) overnight at 4ºC. After rinsing in TBST, the sections were incubated for 15 min with an anti-mouse secondary antibody conjugated to a dextran-labeled polymer and HRP (DakoCytomation K4007), followed by incubation in DAB solution (DakoCytomation DAB #

K4007, Solution 3a, b) for 5 min. The sections were counter-stained with hematoxylin and mounted under cover glasses using a xylene-based mounting medium. GD2 staining scores were assigned as: 0 (negative), 1 (low positive), 2 (moderate positive) and 3 (strong positive). Four cores per case was analyzed. Histoscore was calculated by multiplying the staining intensity by % cells staining. Histoscore distributions were assigned as follows: 0-5, negative; 5-25, low; 25-50, moderate; and >50, strong positive. Histoscore 5 was used as a cut off.

Analysis of *ST8SIA1* mRNA expression in transcriptomic data of CRPC patient-derived xenograft (PDX) tumors and organoid models. *ST8SIA1* mRNA expression was analyzed using publicly-available transcriptomic data on CRPC PDX and organoid models published by Tang et al., (26) (GEO accession GSE199190). As per the author classification, the CRPCs were grouped into 4 groups: Group 1, Androgen Receptor dependent (CRPC-AR); Group 2, Wnt dependent (CRPC-WNT); Group 3, neuroendocrine (CRPC-NE); and Group 4, stem cell like (CRPC-SCL) were analyzed. Gene expression is presented as normalized transcripts per million (TPM).

Cell lines and medium: 22Rv1 and RM-1 cell lines were cultured in RPMI-1640 (Hyclone; #SH30027.02) or DMEM (Gibco; #11965-092), respectively, with 10% fetal bovine serum (Gibco; #10437-028), 10 mM HEPES (Hyclone; #SH30237.01), 1 mM each of sodium pyruvate (Corning; #25-000-CI), nonessential amino acids (Hyclone; #SH30238.01), and L-glutamine (Gibco; #25030-081), 50 μM 2-ME (Gibco; #21985-023), and 1% penicillin/ streptomycin (#15140-122; Gibco). HEK-293T cells (ATCC CRL-3216) were cultured in complete DMEM medium. LNCaP C4-2 parental, p53 stable KD, Rb1 KD cell lines, as well as the parental LNCaP C4-2B and its enzalutamide resistant derivative line (C4-2BER) were grown as described previously (28). Cell lines were maintained for less than 30 days in continuous culture and were regularly tested for mycoplasma.

Reagents and Antibodies: Primary antibodies used for immunoblotting were as follows: anti-ST8SIA1/GD3S from Novus Biologicals (#NBP1-80750) or ProteinTech (#24918-1-AP); anti-SOX2 from ProteinTech (#11064-1-AP); anti-SOX9 from Abcam (#ab185966); anti-Snail from CST (#3879); anti-HSC70 (#sc-7298); anti-p53 (#sc-126), anti-RB1 (#sc-73598) from Santa Cruz Biotechnology; anti-RB1 (BD Bioscience, #554136) and anti-β-actin (#A5441) from Sigma. The horseradish peroxidase (HRP)-conjugated Protein A (#101023) and HRP-conjugated rabbit anti-mouse secondary antibody (#31430) for immunoblotting were from Thermo Fisher. APC conjugated anti-human ganglioside GD2 antibody (#357306; Biolegend) or APC-Mouse-IgG2a,*κ* isotype control (#400220; Biolegend) was used for IHC.

Generation of CRISPR/cas9 knockout and luciferase reporter cell lines: The following constructs were used to generate GD3S KO lines. For mouse RM-1, mouse *St8sia1* sgRNA CRISPR/Cas9 All-in-One Lentivector (pLenti-U6-sgRNA-SFFV-Cas9-2A-Puro; #456551140595, Applied Biological Materials) with three target sequences Target 1-17: GGGCCCTACATACGTCCAGA (sgRNA1), Target 2-56: CTCGGAAATTCCCGCGTACC (sgRNA2), Target 3-141: CTACCGGCTGCCCAACGAGA (sgRNA3). For human 22Rv1 cells, GSGH1195-Edit-R Human All-in-one Lentiviral sgRNA (#GSGH1195-247582548 and #GSGH1195-247725854 designated as sgRNA2 and sgRNA3 respectively) from Horizon Discovery. Lentiviral supernatants generated in Lenti-x HEK-293T cells (TAKARA, #632180) using the 2nd generation packaging system (plasmids psPAX2, Addgene #12260 and pMD2.G, Addgene #12259) were applied to cells for 72h with polybrene (10 µg/ml, Sigma #H9268) and stable lines selected in 2 µg/ml puromycin. Clones obtained by limiting dilution were analyzed by western blotting for GD3S and FACS for GD2. 3 clones for each sgRNA, maintained separately, were pooled for experiments. The tdTomato-luciferase expressing RM-1 cells were generated

using the pMuLE lentiviral system kit (Addgen#1000000060), as described (29). The mCherry-luciferase expressing 22Rv1 derivatives were generated using a lentiviral plasmid (pCDH-EF-eFFly-T2A-mCherry; Addgene #104833). Cell lines with high reporter expression were obtained by FACS sorting.

Western Blotting: Western blotting of whole cell extracts prepared in Triton-X-100 lysis buffer and quantified using the BCA assay kit (#23225; Thermo Fisher Scientific) was performed as described previously (29). 50 µg protein aliquots were run on SDS-7.5% polyacrylamide gels, transferred to polyvinylidene fluoride (PVDF) membrane, and immunoblotted with the indicated antibodies.

Flow cytometry: Cells seeded in regular medium for 48 h were released with trypsin-EDTA (#15400054; LifeTech (ThermoFisher)) and trypsinization stopped with soybean trypsin inhibitor (#17075029; LifeTech (ThermoFisher). Cells were washed thrice in ice-cold FACS buffer (2% FBS, 25mM HEPES in PBS), and live cells stained with APC anti-human GD2 (#357306; Biolegend) (isotype control, APC Mouse IgG2a,κ; #400220, Biolegend) or Anti-human/mouse CD49f antibody (#313620, Biolegend) (isotype control, Pacific Blue Rat IgG2a,κ; #400527, Biolegend). FACS analyses were performed on a BD LSRFortessa X50, BD LSRII or BD LSRII Green instruments and data analyzed using the FlowJo software.

Trans-well migration and invasion assay: Cells grown in 0.5% FBS-containing starvation medium for 24 hours were trypsinized and seeded at 2 x 10^4 on top chambers of 24-well plate trans-wells (Corning, cat# 353097 for migration; or Biocoat Matrigel invasion chambers #354480) in 400 µl of growth factor deprived medium. After 3 hours, medium containing 10% FBS was added to lower chambers and incubated for 16 hours. The non-migrated cells on the upper surface of membranes were removed with cotton swabs, migrated cells on the lower surface were

methanol-fixed and stained in 0.5% crystal violet in methanol. Six random 10x fields per insert were photographed, and cells counted using the ImageJ software. Each experiment was run in triplicates and repeated three times.

Cell proliferation assay: Cell proliferation was assayed as described (29), with 250 cells plated per well in 96-well flat-bottom plates in 100 µl medium and an equal volume of the CellTiter-Glo Luminescent Assay Reagent (#G7571; Promega) added at the indicated time-points. Luminescence was recorded using a GloMax® luminometer (Promega).

Tumorsphere assay: Tumorsphere cultures were done as described (30) with minor modifications. the tumorsphere medium contained DMEM/F12,Thermo Fisher; #1133032) supplemented with 1% penicillin/streptomycin, 4 µg/ml heparin (Stem cell technologies; #07980), 20 ng/ml Animal-Free Recombinant Human EGF (Peprotech; #AF-100-15), 10 ng/ml Recombinant Human FGF-basic (Peprotech; #100-18B), 1X N-2 supplement (Gibco; #17502-048), 1X B27 supplement (Gibco; #17504-044) and 4% Matrigel (BD Biosciences; #356234]. $2x10^4$ cells were seeded per well in 800 ul volume in ultra-low attachment 24-well plates. Tumor-spheres were imaged under a phase contrast microscope after 1 week and quantified using the Image J software. All experiments were done in triplicates and repeated 3 times.

Intra-tibial tumorigenic growth: All animal experiments were performed with the approval of the UNMC Institutional Animal Care and Use Committee (IACUC Protocol# 21-004-06 FC). $4x10^4$ (in 20 µl cold PBS) parental (control) or GD3S-KO (sgRNA1 and sgRNA2) RM-1 cells engineered with lentiviral tdTomato-luciferase or 10^5 (in 40 µl cold PBS) parental (control) or GDS3-KO (sgRNA1) 22Rv1 cells engineered with lentiviral mCherry-enhanced luciferase were injected in tibias of 8-weeks old castrated male C57BL/6 (for RM-1 model) or athymic nude (for 22Rv1 model) mice, respectively, and tumor growth monitored by bioluminescence imaging .

Mice were imaged weekly and followed until the control group reached pre-determined humane end points requiring anesthesia. At necropsy, hind limbs, lungs, spleen, and livers were harvested. For bioluminescence imaging, mice received 200 µl D-luciferin (15 mg/ml; Millipore Sigma #L9504) intraperitoneally 15 min before isoflurane anesthesia and were placed dorso-ventrally in the IVIS™ Imaging System (IVIS 2000). Images were acquired using the IVIS Spectrum CT and analyzed using the Living Image 4.4 software (PerkinElmer). The fold change in total Photon flux (p/s) over time was used to compare tumor growth between the groups.

Bone morphometry analysis: the harvested tibias were fixed in fresh 4% formalin for a day, transferred to 70% ethanol and scanned using a micro-CT scanner (Skyscan 1172, Bruker) (micro-CT scanning core facility, UNMC). The parameters were 55 kV, 593 181 µA, 0.5 mm aluminum filter, 9 µm resolution, 4 frames averaging, 0.4 rotation step, 180° scanning. The images were reconstructed using the NRecon software (version 1.7.4.6, Bruker microCT), registered and realigned using the DataViewer software (version 1.5.6.2, Bruker microCT) and analyzed using the CTAn software (version 1.18.8.0, Bruker microCT) for the percentage of bone volume (BV/TV), trabecular thickness (Tb.Th), trabecular number (Tb.N) and trabecular separation (Tb.Sp).

RNA isolation and Real Time qPCR analysis. Total RNA extracted using the TRIzol® Reagent (Ambion, Life Technology) was converted into cDNA with the Invitrogen SuperScript III system (18080-051) and subjected to real-time qPCR using the SYBR Green labeling method (Applied Biosystems; 4309155) on an Applied Bioscience QuantStudio thermocycler. The primer sequences used were: *ST8SIA1:* (forward) 5′-TCCCAGCATAATTCGGCAA-3′ reverse, 5′-ATCTGACAGTGTATAATAAACCCTC-3′); *B4GALNT1* (forward, 5′-TTCACTATCCGCATAAGACAC-3′; reverse, 5′-GTAACCGTTGGGTAGAAGC-3′);

ST3GAL3 (forward, 5′-ACATTGCTTGTGTTTGGAG-3′; reverse, 5′-GGACGACATTCCTTCTGC-3′); *TP53* (Forward, 5'-CCTCACCATCATCACACTGG-3'; reverse, 5'-CACAAACACGCACCTCAAAG-3'); RB1 (Forward, 5'-CTCTCACCTCCCATGTTGCT-3'; reverse, 5'-GGTGTTCGAGGTGAACCATT-3'); *GAPDH (*forward, 5'-CAGAACATCATCCCTGCCTCT GAPDH; reverse, 5'-GCTTGACAAAGTGGTCGTTGAG GAPDH). The fold change in expression was calculated relative to control (parental) cells using the ΔΔCt method and normalized to GAPDH reference gene expression.

Statistical analysis: GraphPad Prism software (version 9) was used to perform the statistical analyses. The *in vitro* experimental data analysis used a two-tailed student's t test. Two-way ANOVA (mixed model) test was used to analyze the fold change in photon flux in xenograft studies. P values equal to or <0.05 were considered significant.

RESULTS:

Increased GD2 expression upon neuroendocrine differentiation of a CRPC cell line model.

To assess if GD2 overexpression is a feature of PC, we validated a commercially available anti-GD2 antibody (clone 14.G2; Biolegend) for immunostaining of known $GD2^+$ and $GD2^-$ cell lines. FACS as well as immunohistochemistry (IHC) analysis demonstrated that 14.G2 stained the known $GD2^+$ neuroblastoma cell line SK-N-BE-2 (31) but not the $GD2^-$ rhabdomyosarcoma cell line A204 (32), while the isotype control antibody showed similar background staining in both cell lines (**Supplementary Fig. S1**).

We surmised that GD2 overexpression might be a feature of CRPC with neuroendocrine differentiation (CRPC-NE), given the overexpression of GD2 in neuroectodermal lineage tumors

(3), and the known acquisition of CSC features upon CRPC-NE differentiation (33). Depletion of RB1 or TP53 in CRPC-AR cell lines (34) and in mouse models, including when combined with PTEN loss (35), is known to promote the NE trans-differentiation. Therefore, we compared the functional AR-expressing CRPC cell line LNCaP C4-2, which has a mutational inactivation of PTEN (36), with its derivatives with stable knockdown (KD) of TP53 or RB1 (28), with verification of the KD using q-PCR (**Fig. 1B**).The NE differentiation of the KD derivatives has been reported (34,35). FACS staining revealed low cell surface GD2 expression on LNCaP C4-2 cells but a markedly increased GD2-expressing population in RB1- or TP53-KD derivatives (**Fig. 1C**). IHC analyses confirmed these findings (**Fig. 1D**). Increased expression of GD2 upon NE-differentiation of LNCaP C4-2 cells was associated with increase in the expression levels of the key GD2 biosynthesis enzymes, GM3S, GD3S and GD2 synthase (GD2S) (**Fig. 1 E**).

Increased GD2 expression across PC cell lines, including CRPC cell lines driven by diverse mechanisms:

To assess if GD2 was more broadly expressed in PC cell models, we carried out FACS analysis of the cell surface expression of GD2 on a panel of established human and murine PC cell lines, using the LNCaP C4-2 and its RB1 or TP53 KD derivatives characterized above as reference. Among the 18 cell lines analyzed, which included variants of some of the commonly used PC cell lines and two immortal prostate epithelial cell lines (PHPV18 and PSV40), 6 displayed little or no anti-GD2 staining above that with the control antibody **(Table 1, Supplementary Fig. 2A-C**). In contrast, low but clearly detectable levels of GD2 expression on a small subpopulation of cells was observed on 3 PC cell lines (ND1, LNCaP C4-2 and LNCaP C4-2B) and two immortal prostate epithelial cell lines (PHPV18 and PSV40) (**Table 1, Supplementary Fig. 2A-C**). Importantly, a

high proportion of $GD2^+$ cells with high mean fluorescence intensities (MFI's) was observed in the human CRPC cell lines 22Rv1, which overexpresses wildtype AR and ARV7 splice variant (37), and LNCaP C4-2B cells rendered enzalutamide-resistant (28), and on the murine CRPC cell line RM-1 (driven by Ras and Myc) (38) and TRAMP-transgenic mouse-derived TRAMP-C1 cell line (39) (**Table 1, Supplementary Fig. 2A-C**).

The enzyme GD3 synthase (GD3S; encoded by the ST8SIA1 gene) is rate-limiting for GD2 synthesis (2). Consistent with our staining data, the CCLE-DepMap mRNA expression data available for ten PC cell lines showed the highest value for the GD2-high 22Rv1 cell line, and the second lowest value for the GD2-negative PC3 cell line (**Table 1, Supplementary Fig. 2A-C)**. Further analysis of transcriptomics data of CRPC organoids and PDX tumors recently used to classify CRPC into 4 subtypes: CRPC-AR (AR-driven), CRPC-NE (neuroendocrine), CRPC-WNT (WNT pathway-driven) and CRPC-SCL (stem cell like) (26) demonstrated high ST8SIA1 mRNA expression in the FACS-based GD2-high 22Rv1 cell line and nearly undetectable levels in the GD2-negative LNCaP cell line (**Supplementary Fig. S3**). Using the levels in these cell lines as reference, >20% of CRPC organoids and PDX tumors showed increased ST8SIA1 expression, and this was seen across the CRPC subtypes (**Supplementary Fig. S3**). Thus, our results suggested that a majority of established PC cell lines, including examples of CRPC, express low to high GD2 levels on a variable fraction of cells, reminiscent of studies with breast cancer cell models (9,10), and the ST8S1A1 expression results on organoid and PDX models supported the potential of GD2 expression in patient-derived PCs.

GD2 expression is seen on a small subset of tumor cells in primary PC patient tissues and a higher proportion of metastatic lesions.

To assess if GD2 overexpression on a subpopulation of cells in PC cell lines could be extended to human PC we used tissue microarrays (TMAs) from PC patient cohorts. IHC staining of a 320-sample TMA of paired normal prostate tissues and PC samples (Gleason scores of 3-5; from Prostate Cancer Biorepository Network [PCBN]) demonstrated a statistically-significant overexpression of GD2 on primary prostate cancers compared to paired normal prostate tissue (**Fig. 2A-C**); unlike neuroblastoma, with nearly uniform $GD2^+$ tumor cells, but similar to triple-negative breast cancers, only a small subset of tumor cells was $GD2^+$. Overall, about 20% of primary prostate cancers scored GD2+ based on a cutoff of histoscores of less than 5 (**Fig. 2D**). Notably, the IHC analysis of a metastatic PC TMA (the 45-Case Bone and Visceral Metastasis from Rapid Autopsy TMA from PCBN) showed $GD2^+$ staining was seen in about twice the percentage of metastatic lesions compared to primary tumors (**Fig. 2D**). The histoscore distribution analysis showed that metastatic tumors exhibited higher GD2 expression (**Fig. 2E-F**). These results indicate that GD2-expression is a feature of a subpopulation of tumor cells in PC, especially in PC metastasis.

GD2 overexpression defines a PC cell population with higher tumorigenic potential in vitro.

To assess the potential functional role(s) of GD2 overexpression in PC, we first compared the parental LNCaP C4-2 cells (GD2-low) with their RB1- or TP53-KD lines that overexpress GD2. Cell Titer-Glo assays showed that GD2-overexpressing, RB1- or TP53-KD, derivatives exhibited higher and faster cell proliferation (**Fig. 3A**). Transwell migration analyses indicated a higher migratory behavior of GD2-high derivatives compared to C4-2 cells (**Fig. 3B**). Importantly, analyses of 3D tumor-sphere growth under non-attachment conditions, an *in vitro* correlate of CSC

activity (40), demonstrated a marked elevation of tumor-sphere-forming ability of GD2-high RB1- or TP53-KD derivatives as well as C4-2BER compared to LNCaP C4-2 cells (**Fig. 3C**).

Previous studies have shown that GD2-expressing cell fraction is enriched in tumorigenic behaviors (9). We therefore used FACS-sorting to isolate the GD2-high and GD2-low populations of 22Rv1 and RM-1 cell lines which spontaneously express high GD2 on a subpopulation of cells (**Table 1**). Consistent with previous studies demonstrating that GD2 expression is dynamic (41), the FACS-sorted populations re-attained their prior equilibrium with GD2-high and GD2-low populations upon continued culture (**Supplementary Fig. S4)**. Despite the GD2 expression being dynamic, the GD2-high fraction of both 22Rv1 and RM-1 cell lines showed higher tumor-sphere-forming ability (**Fig. 3D**). Further, FACS analysis of 2-D vs. tumor-sphere grown 22RV1 and RM-1 cells showed an enrichment for GD2+ fraction during tumorsphere growth (**Fig. 3E**). Analysis of tumorspheres of both RM-1 and 22Rv1 for CD49f and GD2 dual staining demonstrated that most GD2-postive cells were CD49f-high population compared to GD2-negative population **(Fig. 3F).** These results suggested that GD2-high fraction defines a cell population with higher oncogenic potential and CSC-like behavior.

GD3 synthase, the rate-limiting enzyme in GD2 biosynthesis, is required for *in vitro* oncogenic attributes of GD2-high CRPC cell lines.

In view of our results above, we hypothesized that the $GD2^+$ cell subpopulation is the major driver of the oncogenic attributes of PCs. To test this hypothesis, we targeted the rate-limiting GD2 biosynthesis enzyme GD3S (2) for CRISPR-Cas9 knockout (KO), using a single-vector Cas9/sgRNA expression system, in GD2-overexpressing mouse (RM-1) and human (22Rv1) CRPC cell lines and obtained clonal lines by serial limiting dilution cloning. Western blotting

confirmed the loss of GD3S expression in GD3S sgRNA-targeted derivatives (**Fig. 4A, B**). These GD3S-KO clones indeed lacked the cell surface GD2 expression by FACS analysis (**Fig. 4C, D**). As GD3 is the immediate product of GD3S activity and a precursor of GD2, we also assessed the levels of GD3 in parental vs. GD3S-KO CRPC cell lines, using FACS. Relatively low to modest levels of GD3 were seen on parental cells and this expression was eliminated in KO cells (**Supplementary Fig. S5**).

In both the RM-1 and 22Rv1 cell line models, the GD3S-KO versions exhibited a marked decrease in cell proliferation, migration, and invasion (**Fig. 4 E-H**). GD3S-KO cell lines also exhibited marked impairment of their tumorsphere forming abilities compared to their parental non-targeted cells (**Fig. 5A**), supporting the importance of GD3S and its ganglioside products in promoting the CSC behavior of CRPCs. Further supporting this notion, FACS analysis of GD3S-KO grown cells showed a reduced proportion of CD49f^{hi} cells (**Fig. 5 B**), a marker associated with PC CSCs (42), and western blotting demonstrated markedly reduced levels of EMT markers Snail, N-cadherin, Zeb1, Sox2 and Sox9 in GD3S-KO RM-1 and 22Rv1 cells vs. their control cells **(Fig. 5C).**

GD3S-KO impairs the tumorigenic ability of GD2-high CRPC cell lines.

To assess if the marked reduction in the pro-oncogenic traits upon GD3S-KO observed *in vitro* translates into impaired tumorigenesis *in vivo,* we used lentiviral infection to introduce a tdTomato-luciferase dual reporter into control and GD3S-KO RM-1 cell lines (the latter with two distinct sgRNAs). The tdTomato-high fractions were enriched by FACS-sorting and stable cell lines selected. We implanted the reporter-bearing control and GD3S-KO RM-1 cells in the tibias of castrated syngeneic C57BL/6 mice and monitored tumor growth (5 mice/group) over time by

bioluminescence imaging. While control RM-1 cells generated robust tumors as seen by time-dependent increase in log10 photon flux in IVIS imaging, the GD3S-KO RM-1 cells produced significantly smaller tumors (**Fig. 6A, B**). Reduced tumor growth of GD3S-KO RM-1 implants was confirmed by harvesting the injected limbs (**Fig. 6C**). Morphometric analysis of tibial bone by micro-CT scanning showed reduced bone volume, trabecular number, thickness, and separation in mice implanted with control RM-1 cells, indicative of tumor-induced bone degradation, with a significant amelioration of these defects in tibias of mice implanted with GD3S-KO cells (**Fig. 6D-H**). To confirm these results, we also implanted the mCherry-luciferase expressing parental or GD3S-KO 22Rv1 cells intra-tibially in nude mice and analyzed these by IVIS imaging. Reduced tumorigenesis of GD3S-KO compared to parental tumor cells was confirmed in this model as well by both IVIS imaging (**Fig. 6I, J**) and examination of harvested tumors (**Fig. 6K, L**).

DISCUSSION:

Despite improvements in diagnosis and management of early PC, progression to CRPC and metastatic disease represent lethal transitions responsible for high cancer burden from PC. Identifying targetable molecular pathways that either mark or contribute to these lethal states in PC can open new therapeutic avenues. Here, we use PC patient-derived tumor tissue analyses and as the PC cell line-based mechanistic approaches to demonstrate that the di-ganglioside GD2 marks a small but functionally-critical tumor cell subpopulation in PC with enrichment in more advanced disease states. Our studies using CRPC cell models establish that GD2 contributes to oncogenic drive, thus raising the prospect of GD2 targeting in CRPC using clinically-approved therapeutic agents.

Our analyses of a large cohort of primary and metastatic PC TMAs demonstrated a small subpopulation of tumor cells that expresses GD2, with a significantly higher proportion of

metastatic tumors harboring GD2$^+$ tumor cells (**Fig. 2D**). Notably, while a small percentage of GD2$^+$ cells were seen in normal prostate tissue, the proportion of such cells was significantly higher in tumors (**Fig. 2C**). In this regard, GD2 expression in PC is reminiscent of non-neuroectodermal tumors like breast cancer where only a small proportion of tumor cells express GD2 (9), and the GD2 expression marks the rare stem cell population in normal tissues as well as in tumors (43). No prior studies have examined the GD2 expression at a histological level in PC tissues, but a limited number of prior studies, primarily using biochemical fractionation of glycolipids (22-24), are consistent with our analyses.

Our finding of GD2 expression in a subset of PCs was further substantiated by analyses of a panel of established PC cell lines, with a majority exhibiting GD2 expression on a small to substantial proportion of cells (**Table 1, Supplementary Fig. 2**). Notably, this pattern is similar to that seen in breast and other non-neuroectodermal tumor systems with GD2 expression on a subset of tumor cells (9). The GD2$^+$ and GD2$^-$ populations, however, appear to be in a dynamic equilibrium with each other, as seen by the re-emergence of mixed GD2$^+$/GD2$^-$ populations after the sorted pure GD2$^+$ and GD2$^-$negtaive subsets were cultured *in vitro* (**Supplementary Fig. 4**), similar to that described in other tumor systems (41).

Notably, our analyses of GD2 expression in cell line models demonstrates that GD2 expression can be induced/elevated under scenarios of significance to the evolution of CRPC. First, GD2 could be dramatically induced by experimentally promoting the lineage plasticity of AR$^+$ LNCaP C4-2 CRPC cell line by shRNA KD of TP53 or RB1, both leading to elevated surface levels of GD2 and an increase in the proportion of GD2$^+$ cells (**Fig. 1C**), which was accompanied by a marked elevation in the expression of key GD2 biosynthetic enzymes GD3S and GD2S (**Fig. 1E**). A similar marked induction of GD2 expression was seen when GD2-low LNCaP-C4-2B

CRPC cells were compared to their enzalutamide-resistant derivative LNCaP C4-2BER (28) (**Table 1, Supplementary Fig. S2**). Aside from experimental cell models, our analyses of the expression of the rate-limiting GD2 biosynthetic enzyme GD3S (*St8SIA1*) in publicly-available transcriptomic data on CRPC PDX and tumor-derived organoid models showed that nearly a third of these, across the mechanistic subtypes (26), showed moderate to high GD3S expression (**Supplementary Fig. S3)**. These findings, together with our GD2 staining of primary and metastatic PC TMAs (**Fig. 2A, B, D)**, strongly support the likelihood that our findings are of direct relevance to human CRPC tumors.

The gain of GD2 expression upon genetic (RB1 or TP53 KD) or selection events (enzalutamide resistance) associated with key CRPC progression events (**Fig. 1C, D and Table-1**), and the GD2 expression on a larger proportion of metastatic PC lesions (**Fig. 2D**), supported the likely biological significance of GD2 expression even when expressed on a subset of PC tumor cells. Our results strongly support this notion. Consistent with the $GD2^+$ cell population playing a key role in tumorigenic progression, the TP53- or RB1-KD induced lineage plasticity in LNCaP C4-2 cells markedly elevated their proliferation and tumorsphere forming ability (**Fig. 3A, C**). Importantly, the sorted $GD2^+$ fraction of mouse RM-1 and human 22Rv1 CRPC cell lines was significantly enriched in tumorsphere-forming ability (**Fig. 3D**). Directly establishing the role of GD2, CRISPR-Cas9 KO of GD3S in RM-1 and 22Rv1 cell lines, which eliminated their GD2 expression (**Fig. 4 A-D**), markedly impaired their proliferation, tumorsphere formation, and cell migration/invasion in vitro (**Fig. 4 E-H, Fig. 5A**). Notably, when examined as bone implants in syngeneic (RM-1) or nude mice (22Rv1), the GD3S-KO cell models were markedly impaired for tumorigenesis **(Fig. 6)**.

That GD2 expression on only a subset of tumor cells was nonetheless critical for tumorigenesis is reminiscent of that seen in breast and other cancers, where depletion of GD2 by genetically or pharmacologically downregulating the GD3S expression (11,44) or by immunologically targeting the cell surface GD2 (12) led to impaired tumorigenesis. In these previous studies, GD2 expression has been shown to mark the CSC population, thus accounting for GD2's role in multiple tumorigenic traits. The strong co-staining of GD2 with high CD49f CSC marker (**Fig. 3F**), and the requirements of GD3S for tumorsphere growth (**Fig. 5A**), for the enrichment of the CD49f-high (CSC) population (**Fig. 5B**), and for high EMT marker expression (**Fig. 5C**) are consistent with this idea. However, since our current assignment of a functional role to GD2 expression in PC cell models relied on the GD3S-KO, similar to GD3S depletion employed by others (11,44), it will be important to formally rule out a role of GD3, the other GD3S product and precursor to GD2 (2). Although the surface GD3 levels on the two cell models we targeted for GD3S-KO were relatively modest (**Supplementary Fig. S5**), further immunological targeting of GD2 and/or GD2S depletion should elucidate the functional role of GD2 vs. GD3 in PC tumorigenesis.

Collectively, our findings demonstrate that GD2 overexpression is a feature of a large subset of PCs, that GD2 may be further induced during PC tumor progression, and that the GD2 biosynthetic machinery enzyme GD3S is essential for efficient tumorigenesis in CRPC models. Our findings raise the prospect of anti-GD2 targeting in advanced PC.

ACKNOWLEDGEMENTS

We thank Dr. Ian Frew for Multiple Lentiviral Expression System Kit and Dr. Irmela Jeremias for the pCDH-EF1a-eFFLy-mCherry (mCherry-luciferase reporter) plasmid, obtained through

Addgene. This research was funded by: Pilot grants from the Fred & Pamela Buffett Cancer Center (HB & VB); Department of Defense grants W81XWH-17-1-0616 and W81XWH-20-1-0058 to HB and W81XWH-20-1-0546 to VB; the NIH grants R21CA241055 and R03CA253193 to VB; the NIH Pathway to Independence Award R00 GM1287671 and the NIH MIRA award R35 GM147467 (to M.J.R.); the Raphael Bonita Memorial Fund; and support to UNMC core facilities from the NCI Cancer Center Support Grant (P30CA036727) awarded to Fred & Pamela Buffett Cancer Center and from the Nebraska Research Initiative. AMB, SC and IM received the University of Nebraska Medical Center Graduate Student Fellowships. The content is solely the responsibility of the authors and does not necessarily represent the official views of the NIH, Department of Defense, or other funding agencies.

References:

1. Suzuki M, Cheung NK. Disialoganglioside GD2 as a therapeutic target for human diseases. Expert Opin Ther Targets **2015**;19:349-62
2. Trinchera M, Parini R, Indellicato R, Domenighini R, dall'Olio F. Diseases of ganglioside biosynthesis: An expanding group of congenital disorders of glycosylation. Mol Genet Metab **2018**;124:230-7
3. Nazha B, Inal C, Owonikoko TK. Disialoganglioside GD2 Expression in Solid Tumors and Role as a Target for Cancer Therapy. Front Oncol **2020**;10:1000
4. Cheever MA, Allison JP, Ferris AS, Finn OJ, Hastings BM, Hecht TT*, et al.* The prioritization of cancer antigens: a national cancer institute pilot project for the acceleration of translational research. Clin Cancer Res **2009**;15:5323-37
5. Yu AL, Gilman AL, Ozkaynak MF, London WB, Kreissman SG, Chen HX*, et al.* Anti-GD2 antibody with GM-CSF, interleukin-2, and isotretinoin for neuroblastoma. N Engl J Med **2010**;363:1324-34
6. Dhillon S. Dinutuximab: first global approval. Drugs **2015**;75:923-7
7. Ozkaynak MF, Gilman AL, London WB, Naranjo A, Diccianni MB, Tenney SC*, et al.* A Comprehensive Safety Trial of Chimeric Antibody 14.18 With GM-CSF, IL-2, and Isotretinoin in High-Risk Neuroblastoma Patients Following Myeloablative Therapy: Children's Oncology Group Study ANBL0931. Front Immunol **2018**;9:1355
8. Markham A. Naxitamab: First Approval. Drugs **2021**;81:291-6

9. Battula VL, Shi Y, Evans KW, Wang RY, Spaeth EL, Jacamo RO*, et al.* Ganglioside GD2 identifies breast cancer stem cells and promotes tumorigenesis. J Clin Invest **2012**;122:2066-78

10. Liang YJ, Ding Y, Levery SB, Lobaton M, Handa K, Hakomori SI. Differential expression profiles of glycosphingolipids in human breast cancer stem cells vs. cancer non-stem cells. Proc Natl Acad Sci U S A **2013**;110:4968-73

11. Sarkar TR, Battula VL, Werden SJ, Vijay GV, Ramirez-Pena EQ, Taube JH*, et al.* GD3 synthase regulates epithelial-mesenchymal transition and metastasis in breast cancer. Oncogene **2015**;34:2958-67

12. Ly S, Anand V, El-Dana F, Nguyen K, Cai Y, Cai S*, et al.* Anti-GD2 antibody dinutuximab inhibits triple-negative breast tumor growth by targeting GD2(+) breast cancer stem-like cells. J Immunother Cancer **2021**;9

13. Cheng JY, Hung JT, Lin J, Lo FY, Huang JR, Chiou SP*, et al.* O-Acetyl-GD2 as a Therapeutic Target for Breast Cancer Stem Cells. Front Immunol **2021**;12:791551

14. Chen HC, Joalland N, Bridgeman JS, Alchami FS, Jarry U, Khan MWA*, et al.* Synergistic targeting of breast cancer stem-like cells by human gammadelta T cells and CD8(+) T cells. Immunol Cell Biol **2017**;95:620-9

15. Seitz CM, Schroeder S, Knopf P, Krahl AC, Hau J, Schleicher S*, et al.* GD2-targeted chimeric antigen receptor T cells prevent metastasis formation by elimination of breast cancer stem-like cells. Oncoimmunology **2020**;9:1683345

16. Vantaku V, Donepudi SR, Ambati CR, Jin F, Putluri V, Nguyen K*, et al.* Expression of ganglioside GD2, reprogram the lipid metabolism and EMT phenotype in bladder cancer. Oncotarget **2017**;8:95620-31

17. Yeh SC, Wang PY, Lou YW, Khoo KH, Hsiao M, Hsu TL*, et al.* Glycolipid GD3 and GD3 synthase are key drivers for glioblastoma stem cells and tumorigenicity. Proc Natl Acad Sci U S A **2016**;113:5592-7

18. Sphyris N, Sarkar TR, Battula VL, Andreeff M, Mani SA. GD2 and GD3 synthase: novel drug targets for cancer therapy. Mol Cell Oncol **2015**;2:e975068

19. Shao C, Anand V, Andreeff M, Battula VL. Ganglioside GD2: a novel therapeutic target in triple-negative breast cancer. Ann N Y Acad Sci **2022**;1508:35-53

20. Dalerba P, Cho RW, Clarke MF. Cancer stem cells: models and concepts. Annu Rev Med **2007**;58:267-84

21. Tong D. Unravelling the molecular mechanisms of prostate cancer evolution from genotype to phenotype. Crit Rev Oncol Hematol **2021**;163:103370

22. Satoh M, Fukushi Y, Kawamura S, Ohyama C, Saito S, Orikasa S*, et al.* Glycolipid expression in prostatic tissue and analysis of the antigen recognized by antiprostatic monoclonal antibody APG1. Urol Int **1992**;48:20-4

23. Ravindranath MH, Muthugounder S, Presser N, Selvan SR, Portoukalian J, Brosman S*, et al.* Gangliosides of organ-confined versus metastatic androgen-receptor-negative prostate cancer. Biochem Biophys Res Commun **2004**;324:154-65

24. Ravindranath MH, Muthugounder S, Presser N, Ye X, Brosman S, Morton DL. Endogenous immune response to gangliosides in patients with confined prostate cancer. Int J Cancer **2005**;116:368-77

25. Xing P, Wang Y, Zhang L, Ma C, Lu J. Knockdown of lncRNA MIR44352HG and ST8SIA1 expression inhibits the proliferation, invasion and migration of prostate cancer

cells in vitro and in vivo by blocking the activation of the FAK/AKT/betacatenin signaling pathway. Int J Mol Med **2021**;47

26. Tang F, Xu D, Wang S, Wong CK, Martinez-Fundichely A, Lee CJ*, et al.* Chromatin profiles classify castration-resistant prostate cancers suggesting therapeutic targets. Science **2022**;376:eabe1505

27. Mohapatra BC, Mirza S, Bele A, Gurumurthy CB, Raza M, Saleem I*, et al.* Ecdysoneless overexpression drives mammary tumorigenesis through upregulation of c-MYC and glucose metabolism. Mol Cancer Res **2022**

28. Islam R, Mishra J, Polavaram NS, Bhattacharya S, Hong Z, Bodas S*, et al.* Neuropilin-2 axis in regulating secretory phenotype of neuroendocrine-like prostate cancer cells and its implication in therapy resistance. Cell Rep **2022**;40:111097

29. Luan H, Bielecki TA, Mohapatra BC, Islam N, Mushtaq I, Bhat AM*, et al.* EHD2 overexpression promotes tumorigenesis and metastasis in triple-negative breast cancer by regulating store-operated calcium entry. Elife **2023**;12

30. Wang S, Huang S, Zhao X, Zhang Q, Wu M, Sun F*, et al.* Enrichment of prostate cancer stem cells from primary prostate cancer cultures of biopsy samples. Int J Clin Exp Pathol **2014**;7:184-93

31. Mao Y, Eissler N, Blanc KL, Johnsen JI, Kogner P, Kiessling R. Targeting Suppressive Myeloid Cells Potentiates Checkpoint Inhibitors to Control Spontaneous Neuroblastoma. Clin Cancer Res **2016**;22:3849-59

32. Kailayangiri S, Altvater B, Meltzer J, Pscherer S, Luecke A, Dierkes C*, et al.* The ganglioside antigen G(D2) is surface-expressed in Ewing sarcoma and allows for MHC-independent immune targeting. Br J Cancer **2012**;106:1123-33

33. Conteduca V, Aieta M, Amadori D, De Giorgi U. Neuroendocrine differentiation in prostate cancer: current and emerging therapy strategies. Crit Rev Oncol Hematol **2014**;92:11-24

34. Mu P, Zhang Z, Benelli M, Karthaus WR, Hoover E, Chen CC*, et al.* SOX2 promotes lineage plasticity and antiandrogen resistance in TP53- and RB1-deficient prostate cancer. Science **2017**;355:84-8

35. Ku SY, Rosario S, Wang Y, Mu P, Seshadri M, Goodrich ZW*, et al.* Rb1 and Trp53 cooperate to suppress prostate cancer lineage plasticity, metastasis, and antiandrogen resistance. Science **2017**;355:78-83

36. Vlietstra RJ, van Alewijk DC, Hermans KG, van Steenbrugge GJ, Trapman J. Frequent inactivation of PTEN in prostate cancer cell lines and xenografts. Cancer Res **1998**;58:2720-3

37. Wadosky KM, Ellis L, Goodrich DW. Evasion of targeted cancer therapy through stem-cell-like reprogramming. Mol Cell Oncol **2017**;4:e1291397

38. Baley PA, Yoshida K, Qian W, Sehgal I, Thompson TC. Progression to androgen insensitivity in a novel in vitro mouse model for prostate cancer. J Steroid Biochem Mol Biol **1995**;52:403-13

39. Foster BA, Gingrich JR, Kwon ED, Madias C, Greenberg NM. Characterization of prostatic epithelial cell lines derived from transgenic adenocarcinoma of the mouse prostate (TRAMP) model. Cancer Res **1997**;57:3325-30

40. Liu JC, Deng T, Lehal RS, Kim J, Zacksenhaus E. Identification of tumorsphere- and tumor-initiating cells in HER2/Neu-induced mammary tumors. Cancer Res **2007**;67:8671-81

41. Kroesen M, Nierkens S, Ansems M, Wassink M, Orentas RJ, Boon L*, et al.* A transplantable TH-MYCN transgenic tumor model in C57Bl/6 mice for preclinical immunological studies in neuroblastoma. Int J Cancer **2014**;134:1335-45

42. Goldstein AS, Lawson DA, Cheng D, Sun W, Garraway IP, Witte ON. Trop2 identifies a subpopulation of murine and human prostate basal cells with stem cell characteristics. Proc Natl Acad Sci U S A **2008**;105:20882-7

43. Yanagisawa M. Stem cell glycolipids. Neurochem Res **2011**;36:1623-35

44. Battula VL, Nguyen K, Sun J, Pitner MK, Yuan B, Bartholomeusz C*, et al.* IKK inhibition by BMS-345541 suppresses breast tumorigenesis and metastases by targeting GD2+ cancer stem cells. Oncotarget **2017**;8:36936-49

45. Cao S, Hu X, Ren S, Wang Y, Shao Y, Wu K*, et al.* The biological role and immunotherapy of gangliosides and GD3 synthase in cancers. Front Cell Dev Biol **2023**;11:1076862

Figure Legends:

Fig. 1: **Induction of high GD2 expression in of GD2 in CRPC cell line models with neuroendocrine (NE) differentiation. (A)** Schematic of key GD2 biosynthetic steps displaying the enzymes (*ST3GAL3, ST8SIA1* and *B4GALNT1*) and intermediate products (GM3 and GD3) [Adapted from (45)]. LNCaP C4-2 cells with stable knockdown (KD) of p53 or RB1, previously shown to undergo NE differentiation, were compared with parental cells. **(B)** qPCR analysis for *TP53* and *RB1* mRNA expression shows p53 or Rb1 KD cells relative to LNCaP C4-2 cells. Data represent mean ± SEM with two-tailed unpaired *t* test. n = 3; ***, $P < 0.001$. (C) Cell surface GD2 expression analyzed by live cell surface staining with anti-GD2 vs isotype control antibodies followed by flow cytometry. X-axis, fluorescence intensity; Y-axis, Events normalized to mode. FACS plots display % cells staining positive and mean fluorescence intensity (MFI) of staining with anti-GD2 (cyan) and isotype control (red). (D) Immunohistochemistry (IHC) staining confirmation of increased GD2 expression on TP53- or RB1-knockdown LNCaP-C4-2 cells relative to parental cells. **(E)** qPCR analysis shows increased expression of *ST3GAL3, ST8SIA1* and *B4GALNT1 mRNAs* in p53 KD *and* RB1 KD cells compared to parental LNCaP C4-2 cell line. Data are mean ± SEM with two-tailed unpaired *t* test. n = 3; *, $P < 0.05$.

Fig. 2: GD2 expression on a subset of tumor cells in primary prostate cancer tissue with higher expression in metastatic lesions. Tissue microarrays (TMAs) composed of paired normal prostate and prostate cancer Gleason grades (3, 4 and 5) (n = 320) or 45 cases of bone and visceral metastatic samples (both obtained from the Prostate Cancer Biorepository Network) were analyzed by IHC staining for GD2. Histoscores were calculated by multiplying the staining intensity (0, negative; 1, low; 2, moderate positive; 3, strong positive) by the % tumor cells staining positive.

(**A, B**) Representative examples of negative, low, moderate, and high GD2 staining in primary (**A**) and metastatic (**B**) tumor samples. (**C**) Scattered plot shows histoscore distribution of primary tumors and normal prostate. GD2 expression is significantly higher in primary tumors than normal prostate. Data represents 34 cases of GD2 expression in tumors vs 24 in normal tissue, considering histoscore >25 as positive. Mann-Whitney unpaired t-test used as statistical analysis; *, $P < 0.05$. **(D)** Pie charts displaying the % of cases that were GD2+ or GD2-negative in primary and metastatic tumors samples. Histoscores of 0-5 were considered negative while scores higher than 5 were considered positive. (**E, F**) Frequency distribution plots histoscores plotted against percentage of patients (**E**) and number (**F**) of patients. The indicated histoscore grouping are: 0-5 (negative); 5-25 (low), 25-50 (moderate); and >50 (strong).

Fig. 3: GD2 overexpression promotes the *in vitro* oncogenic traits: (**A**) Analysis of cell proliferation. The parental LNCaP C4-2 and its *TP53* KD or *RB1* KD cells were plated in 96-well plates and cell proliferation was assessed on the indicated days (Day 1 to Day 5) using the CellTiter-Glo luminescent cell viability assay. The Y-axis represents the fold increase in relative luminescence units (RLU) relative to Day 1. Data are mean ± SEM with analysis by multiple unpaired *t* test. n = 3 with six replicates each; **, $P < 0.01$; ***, $P < 0.001$. (**B**) Analysis of cell migration. 20,000 parental, *TP53* KD or *RB1* KD cells plated in low serum medium in top chambers of trans-well chambers were allowed to migrate for 3 hours towards serum-containing medium in the bottom chambers. Left, representative images. Right, quantification. Data represent mean ± SEM with unpaired t test. n = 3 with three replicates each; ***, $P < 0.001$. (**C**) Analysis of tumorsphere forming ability. The indicated cell lines were plated in 24-well ultra-low attachment plates in 4% Matrigel and images were obtained on Day 7. Left, representative images; scale bar, 1000 µm. Right, quantified tumorsphere numbers per 4x microscopic field. . Data represent mean

± SEM with unpaired t test. n = 3 with three replicates each and 6 images per well; ***, $P < 0.001$. (**D**) GD2+ fraction of CRPC cell lines is enriched for tumorsphere-forming ability. Constitutively GD2-expressing RM-1 and 22Rv1 CRPC cell lines were FACS sorted for $GD2^-$ and $GD2^+$ populations, grown on 2D overnight and plated at 20,000 cells per well of 24-well ultra-low attachment plates in tumorsphere media containing 4% Matrigel. Tumor-spheres were imaged on Day 5. Left, representative images. Right, Quantification of tumorspheres (>250 μm) per 4X magnification filed. Data represent mean ± SEM with unpaired t test. n = 3 with three replicates each and 6 images per well; ns, not significant; **, $P < 0.01$; ***, $P < 0.001$**.** (**E**) Enrichment of GD2+ cells in tumorspheres of CRPC cell lines. The indicated cell lines were cultured on plastic in regular two-dimensional (2D) cultures or were seeded in tumorsphere cultures. Cells harvested at the indicated times were analyzed for cell surface GD2 expression (vs. isotype control) at the indicated times. % GD2+ cells and MFI are indicated. Left, representative FACS images; Right, quantitation of data. Mean ± SEM with two-way ANOVA test, **, $P < 0.01$; ***, $P < 0.001$**.** **(F)** FACS analysis of tumorsphere-grown RM-1 and 22Rv1 cell lines after anti-GD2 and anti-CD49f double-staining shows a majority of GD2+ cells to be CD49f-high. % GD2 and/or CD49f negative/positive populations is shown in the respective quadrants.

Fig. 4: *GD3S* knockout in CRPC cell lines impairs the in vitro tumorigenic and pro-metastatic traits. (**A-D**) Generation of **GD**3S knockout of RM-1 and 22Rv1 CRPC cell lines. Cells were transduced with lentiviral All-in-One CRISPR/Cas9 constructs and stable clones analyzed by Western blotting with anti-GD3S antibody; Hsc70, loading control. Known GD2+ (9464D) and GD2- (975A2) mouse neuroblastoma cell lines were used as and controls. (**C-D**) Complete loss of cell surface GD2 expression in GD3S-KO RM-1 and 22Rv1 clones. The parental cell lines and their GD3S-KO clones were live cell stained with anti-GD2 (blue) or isotype control

(red) antibody followed by FACS analysis. FACS plots indicate mean fluorescence intensity (MFI) on X-axis vs. Events Normalized to Mode on Y-axis. % positive cells and MFIs are indicated in FACS plots. (**E-F**) Reduced CRPC cell proliferation upon GD3S-KO. Three clones of parental and GD3S-KO cell lines maintained separately were mixed plated at 1,000 cells per well in 96-well plates and live cells quantified at the indicated times using the CellTiter-Glo cell viability assay. The Y-axis represents the fold increase in relative luminescence units (RLU) relative to Day 1. Data are mean ± SEM with analysis by multiple unpaired t test. n = 3 with six replicates each; *p<0.05, **p<0.01. (**G-H**) Reduced CRPC cell migration (**G**) and invasion (**H**) upon GD3S-KO. 20,000 parental or GD3S-KO RM-1 or 22Rv1 cells were plated in low serum medium in top chambers of trans-well chambers without (migration) or with (invasion) Matrigel coating and allowed to migrate or invade for 16 hours towards serum-containing medium in the bottom chambers. Left, representative images. Right, quantification. Data represent mean ± SEM with unpaired *t* test. n = 3 with three replicates each and 6 images per well; ; ***p<0.001. (**I-J**) Reduced CRPC tumorsphere forming ability upon GD3S-KO. The indicated cell lines were plated in 24-well ultra-low attachment plates in 4% Matrigel and images were obtained on Day 7. Left, representative images; scale bar, 1000 µm. Right, quantified tumorsphere numbers per 4x microscopic field. Data represent mean ± SEM with unpaired *t* test. n = 3 with three replicates each and 6 images per well; , unpaired *t-test* ; ***p<0.001.

Fig. 5: Impairment of cancer stem cell (CSC)-associated traits in CRPC cell lines upon GD3S-KO. (**A**) Reduced CRPC tumorsphere forming ability upon GD3S-KO. The indicated cell lines were plated in 24-well ultra-low attachment plates in 4% Matrigel and images were obtained on Day 7. Left, representative images; scale bar, 1000 µm. Right, quantified tumorsphere numbers

per 4x microscopic field. Data represent mean ± SEM with unpaired t test. n = 3 with three replicates each and 6 images per well; unpaired *t-test* ; ***p<0.001. **(B)** Reduced expression of CSCs markers in GD3S-KO CRPC cell lines. The indicated cell lines were subjected to live cell staining followed by Left, representative FACS plots display CD49F staining (MFI's) on X-axis and forward scatter on Y-axis. Right, quantitation of % of CD49f-high population. Data are mean ± SEM, unpaired *t test*; n=3; *p<0.05, **p<0.01. (**C**) Reduced expression of Epithelial-Mesenchymal Transition (EMT) markers in GD3S-KO CRPC cell lines. Lysates of the parental vs. GD3S-KO RM-1 or 22Rv1 cell lines were subjected to western blotting with antibodies against Snail, N-cadherin, ZEB1, SOX2 and SOX9, with Hsc70 or β-actin used as loading controls. Densitometric quantification is shown on top of each blot.

Fig. 6: Impairment of in vivo bone-implanted CRPC tumorigenesis by GD3S KO. (**A**) Parental (Control) RM-1 cells or their edited versions carrying sgRNA1 or sgRNA2 (GD3S-KO) were engineered with tdTomato-luciferase and 4 x 10^4 cells injected in tibias of castrated male C57/BL6 mice (8/group) and primary tumor growth was monitored by bioluminescence imaging at the indicated time points in mice (5/group) with detectable bioluminescent signals on day 8. (**B**) Bioluminescence signals of RM-1 tumors over time are shown as log fold-change in photon flux over the time. Data are mean ± SEM, n=5; Two-way ANOVA (mixed model); *p<0.05. (**C**) Photographs of RM-1 tumor-bearing limbs harvested from control and GD3S-KO cell impalnted groups are displayed. The blue circle represents the tumor area in the tibia. (**D**) Micro-CT scanned images of tibias isolated from mice implanted with the indicated RM-1 cell lines. μCT analyses of the trabecular bone was used to calculate the: (**E**) bone volume fraction (BV/TV%); (**F**) trabecular thickness (μm); (**G**) trabecular number (per μm); and (**H**) trabecular separation (μm). Data

represent mean ± SEM, with unpaired t-test used for statistical analysis; *p<0.05 and ** p<0.01. (**I**) Impairment of tumorigenesis of 22Rv1 CRPC cells by GD3S-KO. 2 x 10^5 control or GD3S KO (sgRNA1) 22Rv1 cells engineered with mCherry-luciferase were injected in tibias of castrated male athymic nude mice (6/group) and tumor growth was monitored by bioluminescence imaging in mice (5/group) with detectable bioluminescent signals on day. (**J**) Bioluminescence signals of 22Rv1 xenografts over time are shown as log fold-change in photon flux over time. Data are mean ± SEM, n=6, with analysis by Two-way ANOVA (mixed model); **p<0.01. (**K**) Quantification of harvested tumor weights (tumor-bearing limb minus contralateral noninjected limb weight). Data represents mean ± SEM, n=6; unpaired t-test showed the significant differences between Control vs GD3S KO groups (*p<0.05). (**L**) Photographs of 22Rv1 tumor-bearing limbs harvested from control and GD3S-KO cell implanted groups are displayed.

Supplementary Figure Legends:

Fig. S1. Validation of anti-GD2 antibody. (A) FACS analysis of GD2-negative A-204 Rhabdomyosarcoma and GD2+ SK-N-BE(2) human neuroblastoma cell lines stained with anti-GD2 vs. no primary antibody (unstained cells). (B) Immunohistochemistry (IHC) staining of A-204 and SK-N-BE(2) cell lines with anti-GD2 or isotype control. Scale bar, 50 µm. Insets show a higher magnification of regions within each image. GD2 antibody selectively stains the SK-NB-2 but not the A-204 cell line.

Fig. S2: FACS plots of cell surface GD2 expression on human and mouse prostate cancer (PC) cell lines. he indicated human and mouse prostate cancer cell lines were live-cell stained using anti-GD2 vs. isotype control and analyzed by FACS. GD2, cyan; isotype control, red. Percentage % population and MFI are indicated in FACS plots. (**A**) Cell lines with essentially

undetectable GD2 (all human). (**B**) GD2-low PC cell lines (all human). (**C**) GD2-high human (22Rv1 and LNCaP C4-2BER) and mouse PC cell lines (RM-1 and Tramp-C1) are shown.

Fig. S3: High *ST8SIA1* (GD3S) mRNA expression in a substantial proportion of CRPC patient-derived xenograft (PDX) tumors and organoid models. Publicly available transcriptomic data published by Tang et al.(26) (GEO accession GSE199190) on CRPC PDX and organoid models were queried for *ST8SIA1* mRNA expression. The CRPC groups are as per Tang et al: Group 1, Androgen Receptor dependent (CRPC-AR, peach); Group 2, Wnt dependent (CRPC-WNT, green); Group 3, neuroendocrine (CRPC-NE, blue); and Group 4, stem cell like (CRPC-SCLm purple). Gene expression is shown as normalized transcripts per million (TPM). The horizontal red line in left panel demarcates the negative/positive cutoff based on $GD2^-$ LNCaP cells.

Fig. S4: Re-expression of GD2-positive population from GD2-negative cells:

(A, B) GD2-positive and GD2-negative population were FACS sorted in RM-1 and 22RV1 cells and grown as 2D and tumorspheres. After Day 5, the cells were reanalyzed for GD2 fractions in both GD2+ and GD2-negative post sorted cells. In both tumorspheres and 2D culture the GD2-negative cells re-expressed GD2. Blue arrows indicate the FACS plots of GD2-negative or GD2-positive cells.

Fig. S5: FACS plots of cell surface GD2 expression on human and mouse prostate cancer (PC) cell lines. he indicated human and mouse prostate cancer cell lines were live cell stained using anti-GD2 vs. isotype control and analyzed by FACS. GD2, cyan; isotype control, red. Percentage % population and MFI are indicated in FACS plots. (**A**) Cell lines with essentially

undetectable GD2 (all human). (**B**) GD2-low PC cell lines (all human). (**C**) GD2-high human (22Rv1 and LNCaP C-4-2BER) and mouse PC cell lines (RM-1 and Tramp-C1) are shown.

Fig. 1

A.

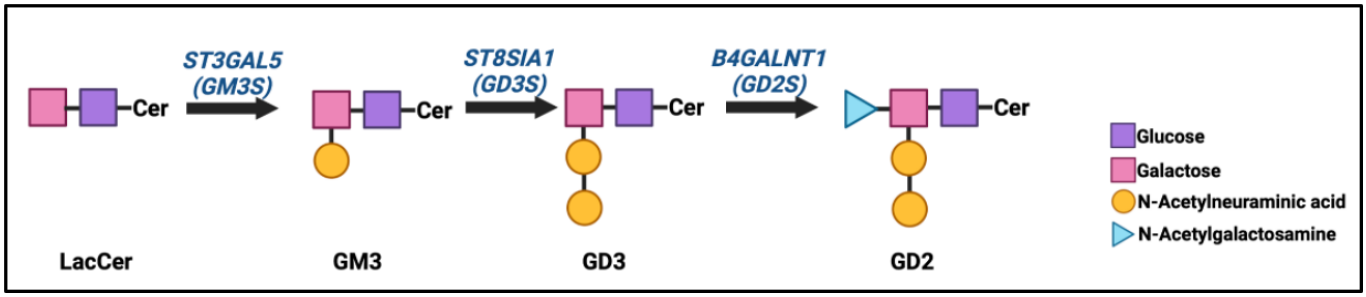
ST3GAL5
(GM3S)
ST8SIA1
(GD3S)
B4GALNT1
(GD2S)
Cer
LacCer
GM3
GD3
GD2
Glucose
Galactose
N-Acetylneuraminic acid
N-Acetylgalactosamine

B.

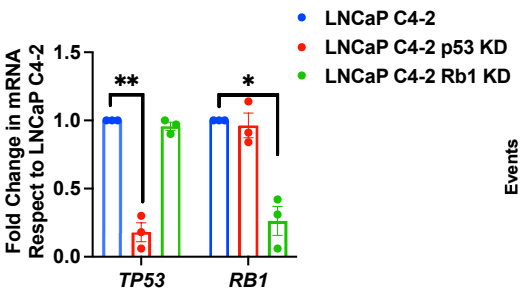
LNCaP C4-2
LNCaP C4-2 p53 KD
LNCaP C4-2 Rb1 KD
Fold Change in mRNA
Respect to LNCaP C4-2
1.5
1.0
0.5
0.0
**
*
TP53
RB1

C

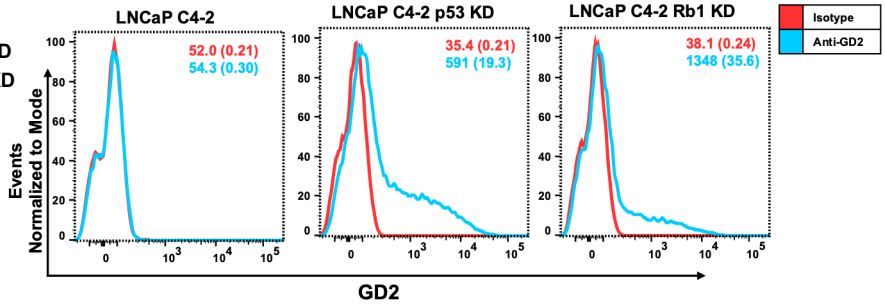
LNCaP C4-2
LNCaP C4-2 p53 KD
LNCaP C4-2 Rb1 KD
Isotype
Anti-GD2
52.0 (0.21)
54.3 (0.30)
35.4 (0.21)
591 (19.3)
38.1 (0.24)
1348 (35.6)
Events
Normalized to Mode
GD2

D

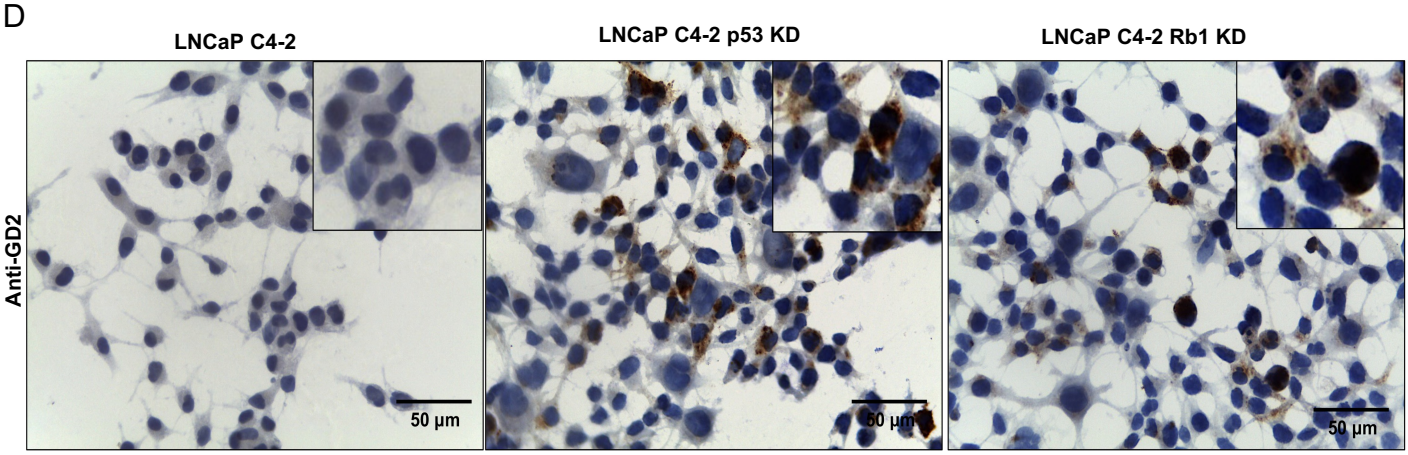
LNCaP C4-2
LNCaP C4-2 p53 KD
LNCaP C4-2 Rb1 KD
Anti-GD2
50 µm
50 µm
50 µm

E

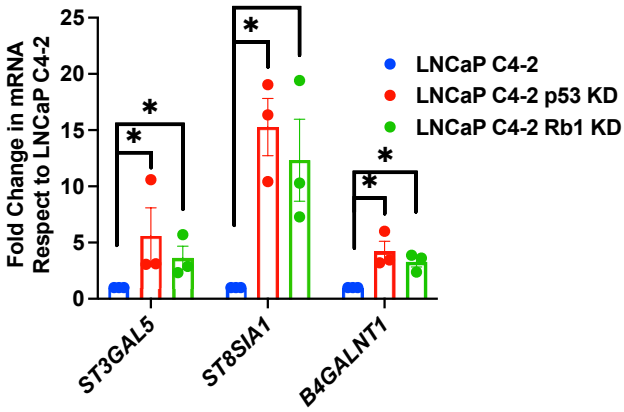
LNCaP C4-2
LNCaP C4-2 p53 KD
LNCaP C4-2 Rb1 KD
Fold Change in mRNA
Respect to LNCaP C4-2
25
20
15
10
5
0
*
ST3GAL5
ST8SIA1
B4GALNT1

Fig. 2

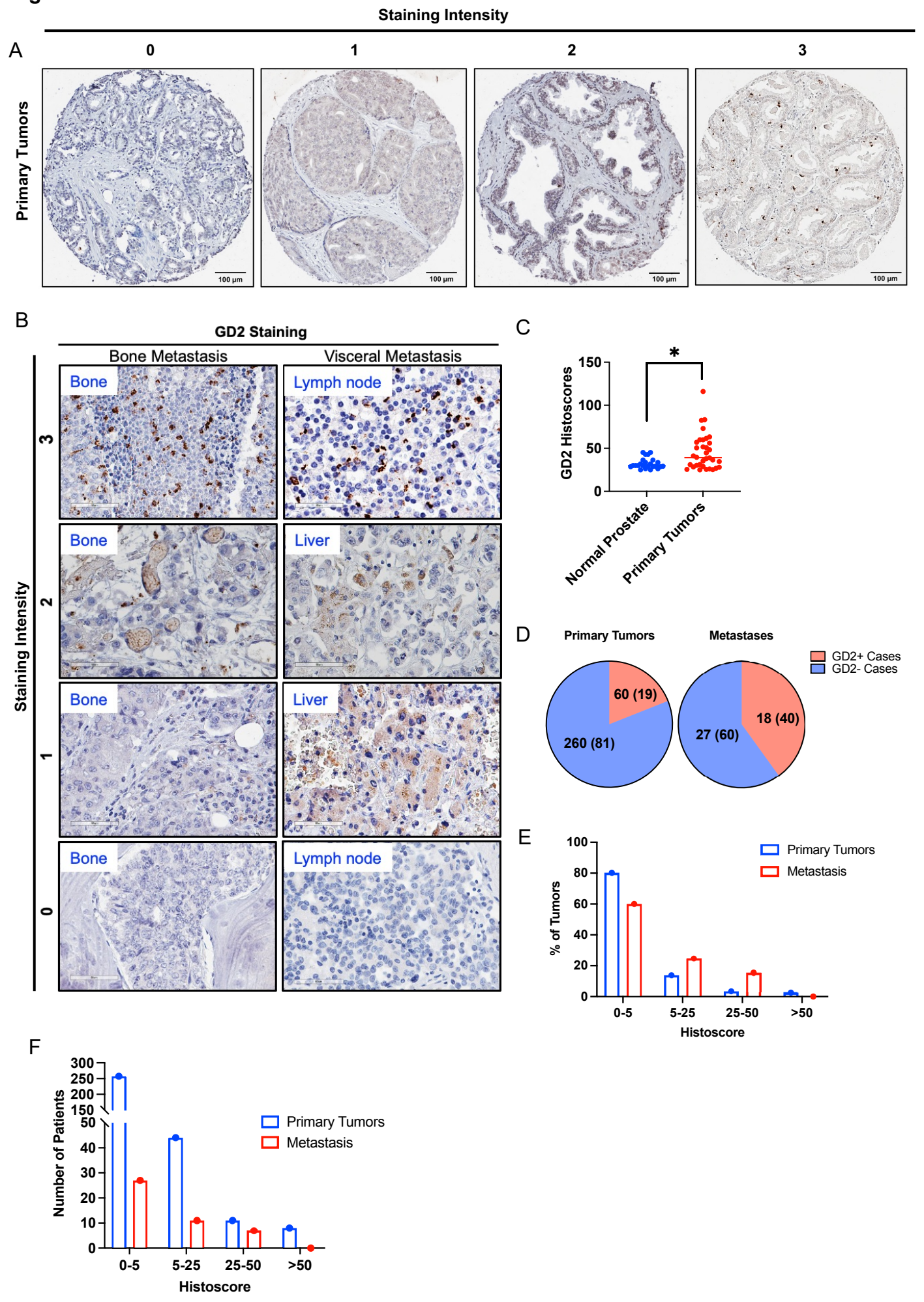
Staining Intensity
A
0
1
2
3
Primary Tumors
100 µm
B
GD2 Staining
Bone Metastasis
Visceral Metastasis
Staining Intensity
Bone
Lymph node
Liver
C
GD2 Histoscores
150
100
50
0
*
Normal Prostate
Primary Tumors
D
Primary Tumors
Metastases
GD2+ Cases
GD2- Cases
60 (19)
260 (81)
18 (40)
27 (60)
E
% of Tumors
Primary Tumors
Metastasis
0-5
5-25
25-50
>50
Histoscore
F
Number of Patients
Primary Tumors
Metastasis
0-5
5-25
25-50
>50
Histoscore

Fig. 3

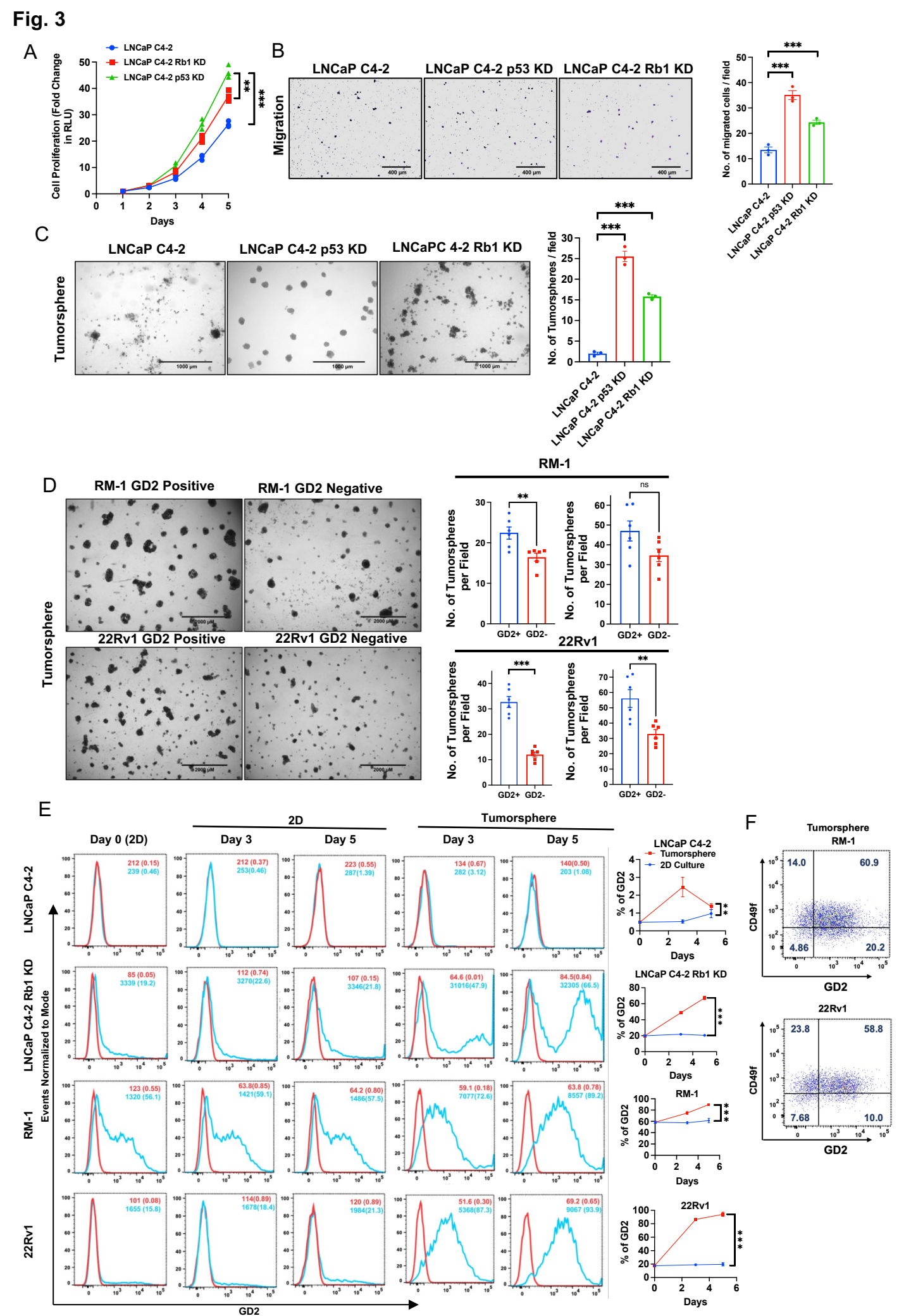
A
LNCaP C4-2
LNCaP C4-2 Rb1 KD
LNCaP C4-2 p53 KD
Cell Proliferation (Fold Change in RLU)
Days
B
Migration
LNCaP C4-2
LNCaP C4-2 p53 KD
LNCaP C4-2 Rb1 KD
No. of migrated cells / field
C
Tumorsphere
LNCaP C4-2
LNCaP C4-2 p53 KD
LNCaPC 4-2 Rb1 KD
No. of Tumorspheres / field
D
Tumorsphere
RM-1 GD2 Positive
RM-1 GD2 Negative
22Rv1 GD2 Positive
22Rv1 GD2 Negative
RM-1
22Rv1
No. of Tumorspheres per Field
GD2+
GD2-
ns
E
2D
Tumorsphere
Day 0 (2D)
Day 3
Day 5
LNCaP C4-2
LNCaP C4-2 Rb1 KD
RM-1
22Rv1
Events Normalized to Mode
GD2
Tumorsphere
2D Culture
% of GD2
Days
F
Tumorsphere
RM-1
22Rv1
CD49f
GD2

Fig. 4

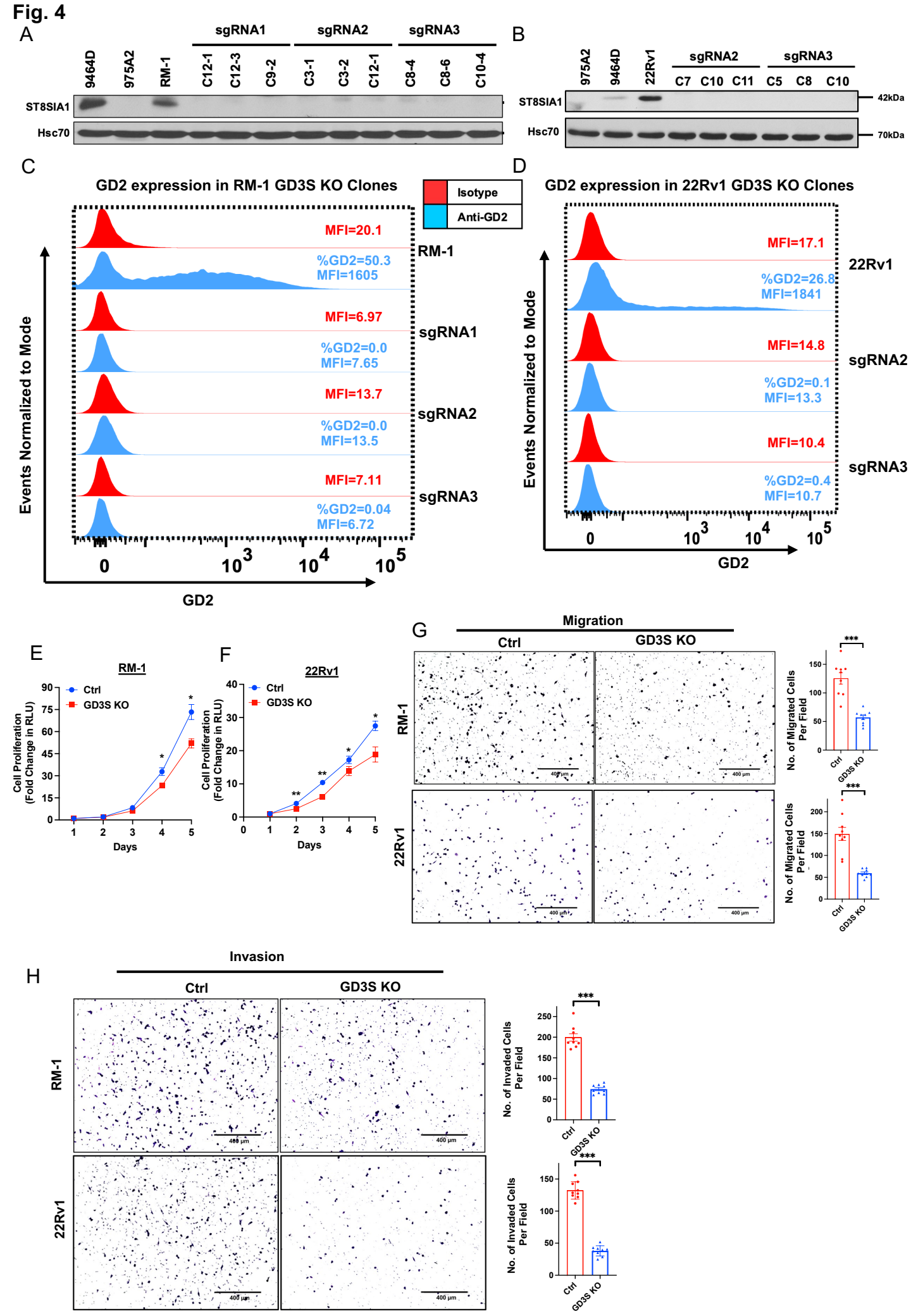
A
sgRNA1
sgRNA2
sgRNA3
9464D
975A2
RM-1
C12-1
C12-3
C9-2
C3-1
C3-2
C12-1
C8-4
C8-6
C10-4
ST8SIA1
Hsc70
B
975A2
9464D
22Rv1
sgRNA2
C7 C10 C11
sgRNA3
C5 C8 C10
ST8SIA1
Hsc70
42kDa
70kDa
C
GD2 expression in RM-1 GD3S KO Clones
Isotype
Anti-GD2
MFI=20.1
%GD2=50.3
MFI=1605
RM-1
MFI=6.97
%GD2=0.0
MFI=7.65
sgRNA1
MFI=13.7
%GD2=0.0
MFI=13.5
sgRNA2
MFI=7.11
%GD2=0.04
MFI=6.72
sgRNA3
Events Normalized to Mode
0
10^3
10^4
10^5
GD2
D
GD2 expression in 22Rv1 GD3S KO Clones
MFI=17.1
%GD2=26.8
MFI=1841
22Rv1
MFI=14.8
%GD2=0.1
MFI=13.3
sgRNA2
MFI=10.4
%GD2=0.4
MFI=10.7
sgRNA3
Events Normalized to Mode
0
10^3
10^4
10^5
GD2
E
RM-1
Ctrl
GD3S KO
Cell Proliferation (Fold Change in RLU)
Days
F
22Rv1
Ctrl
GD3S KO
Cell Proliferation (Fold Change in RLU)
Days
G
Migration
Ctrl
GD3S KO
RM-1
22Rv1
400 µm
No. of Migrated Cells Per Field
Ctrl
GD3S KO
H
Invasion
Ctrl
GD3S KO
RM-1
22Rv1
400 µm
No. of Invaded Cells Per Field
Ctrl
GD3S KO

Fig. 5

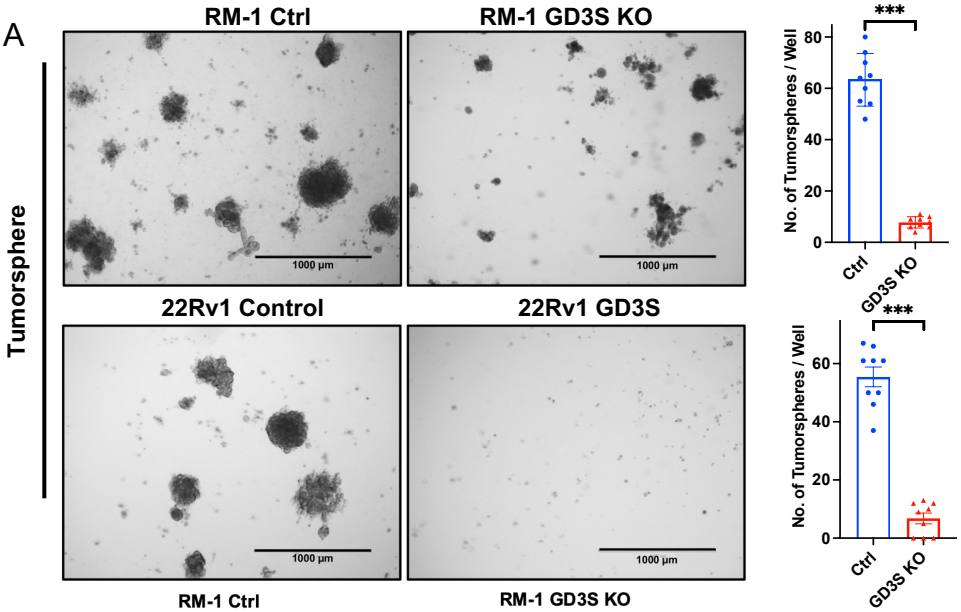
A
Tumorsphere
RM-1 Ctrl
RM-1 GD3S KO
22Rv1 Control
22Rv1 GD3S
1000 µm
No. of Tumorspheres / Well
Ctrl
GD3S KO
***

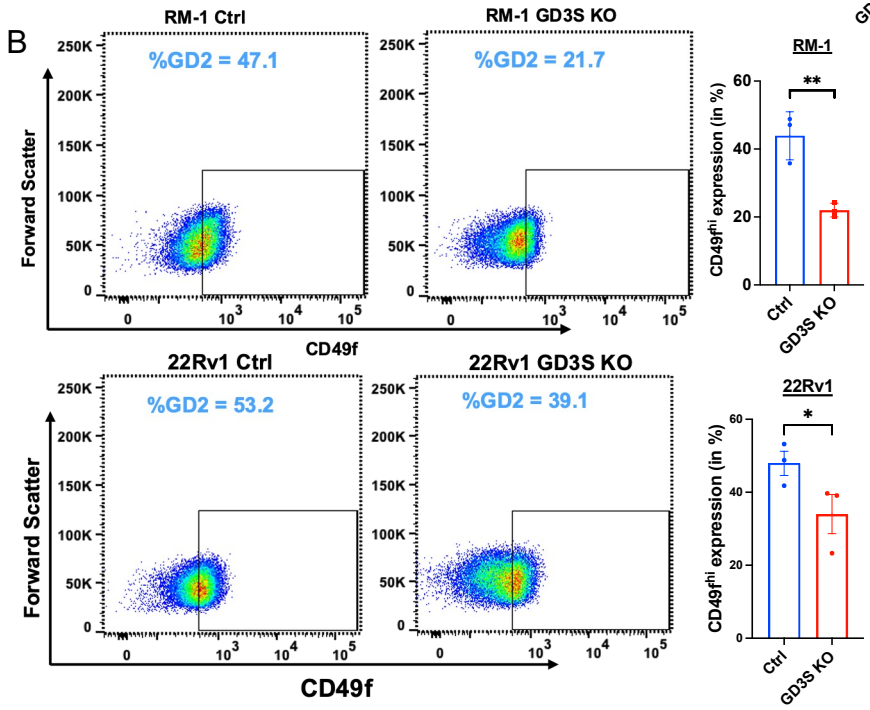
B
RM-1 Ctrl
RM-1 GD3S KO
%GD2 = 47.1
%GD2 = 21.7
22Rv1 Ctrl
22Rv1 GD3S KO
%GD2 = 53.2
%GD2 = 39.1
Forward Scatter
CD49f
CD49f^hi expression (in %)
RM-1
22Rv1
Ctrl
GD3S KO
**
*

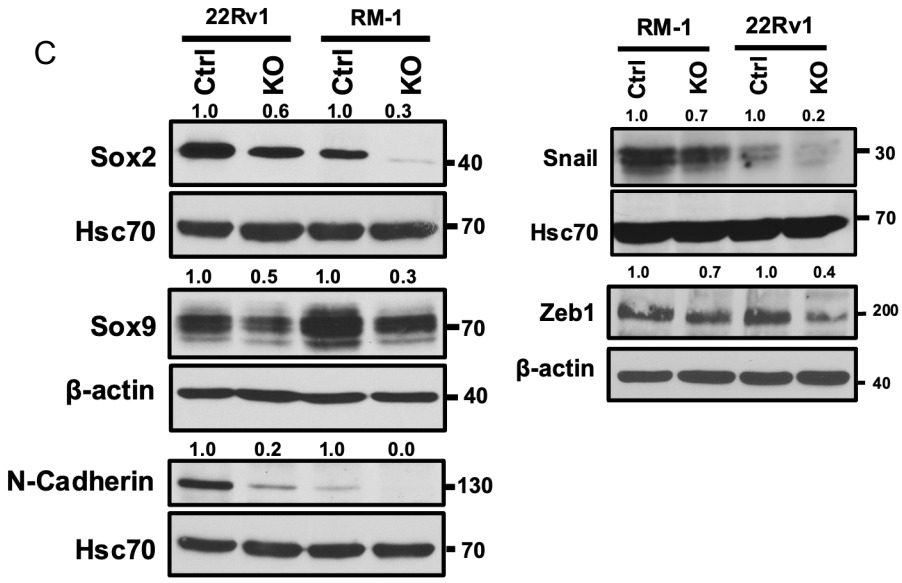
C
22Rv1
RM-1
Ctrl
KO
Sox2
Hsc70
Sox9
β-actin
N-Cadherin
Snail
Zeb1
1.0 0.6 1.0 0.3
1.0 0.5 1.0 0.3
1.0 0.2 1.0 0.0
1.0 0.7 1.0 0.2
1.0 0.7 1.0 0.4
40
70
130
30
200

Fig. 6

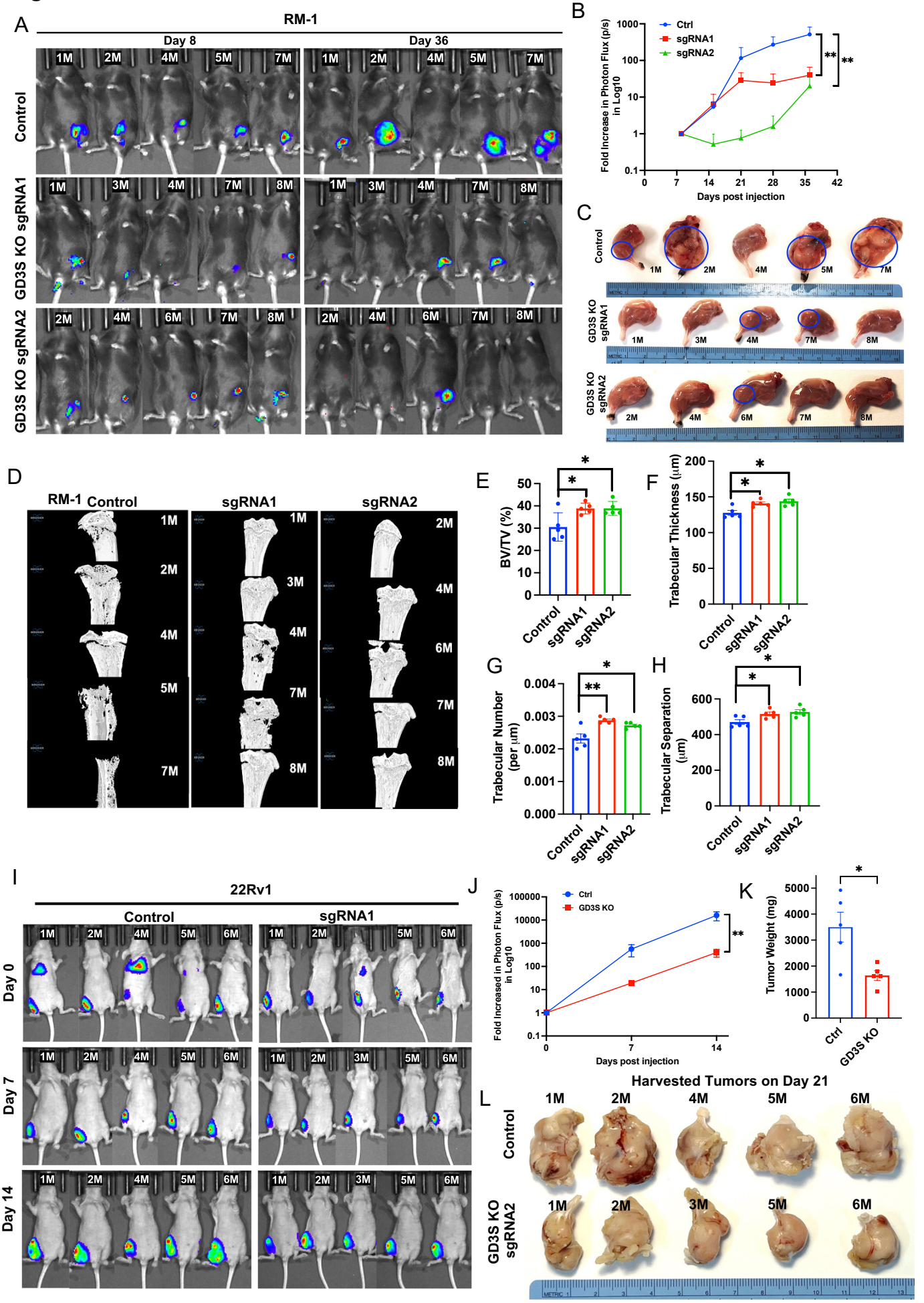
A
RM-1
Day 8
Day 36
Control
GD3S KO sgRNA1
GD3S KO sgRNA2
B
Ctrl
sgRNA1
sgRNA2
Fold Increase in Photon Flux (p/s) in Log10
Days post injection
C
Control
GD3S KO sgRNA1
GD3S KO sgRNA2
D
RM-1 Control
sgRNA1
sgRNA2
E
BV/TV (%)
F
Trabecular Thickness (μm)
G
Trabecular Number (per μm)
H
Trabecular Separation (μm)
Control
sgRNA1
sgRNA2
I
22Rv1
Control
sgRNA1
Day 0
Day 7
Day 14
J
Ctrl
GD3S KO
Fold Increased in Photon Flux (p/s) in Log10
Days post injection
K
Tumor Weight (mg)
Ctrl
GD3S KO
L
Harvested Tumors on Day 21
Control
GD3S KO sgRNA2

Table-1: Prostate cancer cell lines show % GD2 on live cell FACS analysis using anti-GD2 staining.

Cell Line Names	% GD2
PC3	0
PC3M	0
PC3M LN4	0
LNCaP (Low Passage)	0
MDA PCa2b (Low Passage)	0
NE1.3	0
DU145	0
ND1	~0 - 2
LNCaP C4-2	~0 - 2
LNCaP C4-2B	~0 - 2
PHPV18	~2 - 3
PSV40	~4 - 6
22Rv1	~15 - 30
LNCaP C4-2 RB1 KD	~10 - 20
LNCaP C4-2 p53 KD	~10 - 35
LNCaP C4-2BER (Enzalutamide Resistant)	~25 - 40
TRAMP-C1	~40 - 60
RM-1	~45 - 70

Supplementary Figures

Supplementary Fig. S1.

A.

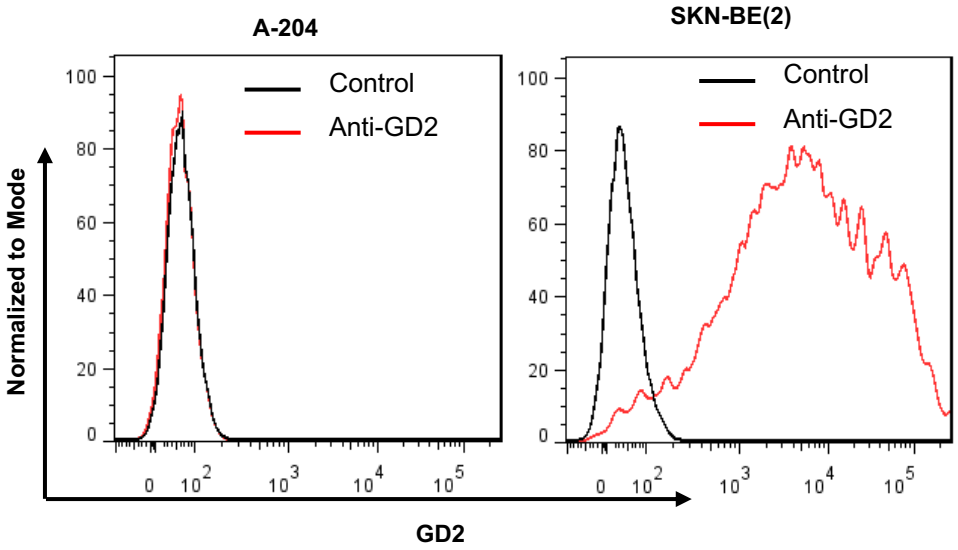

B.

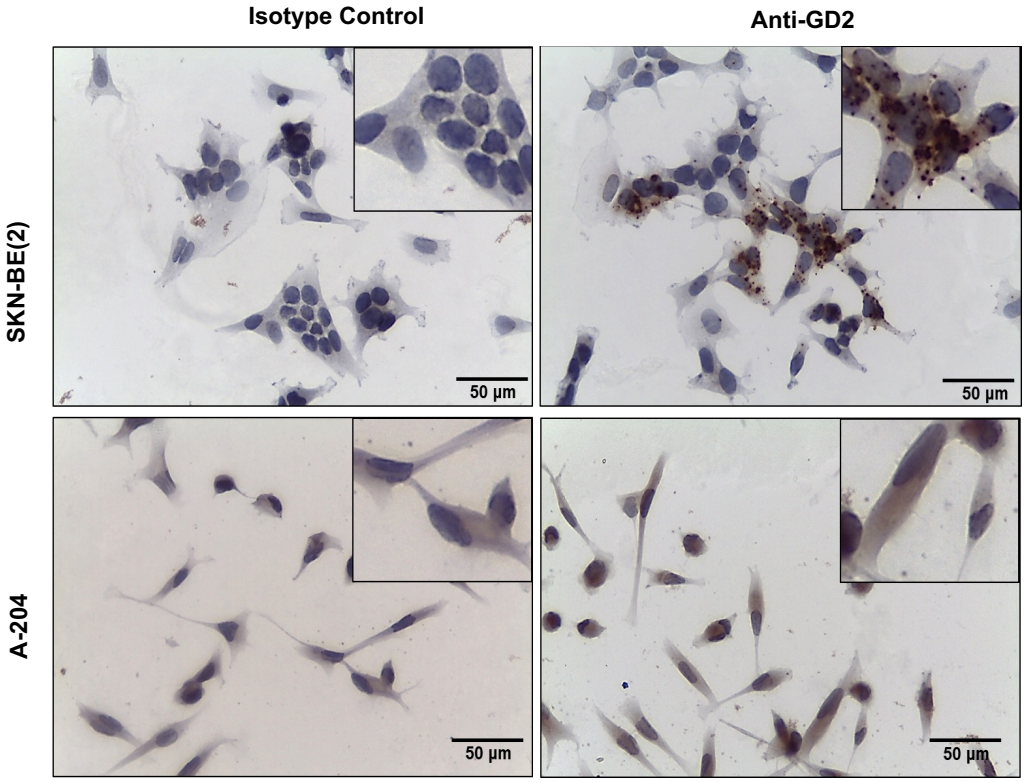

Supplementary Fig. S2.

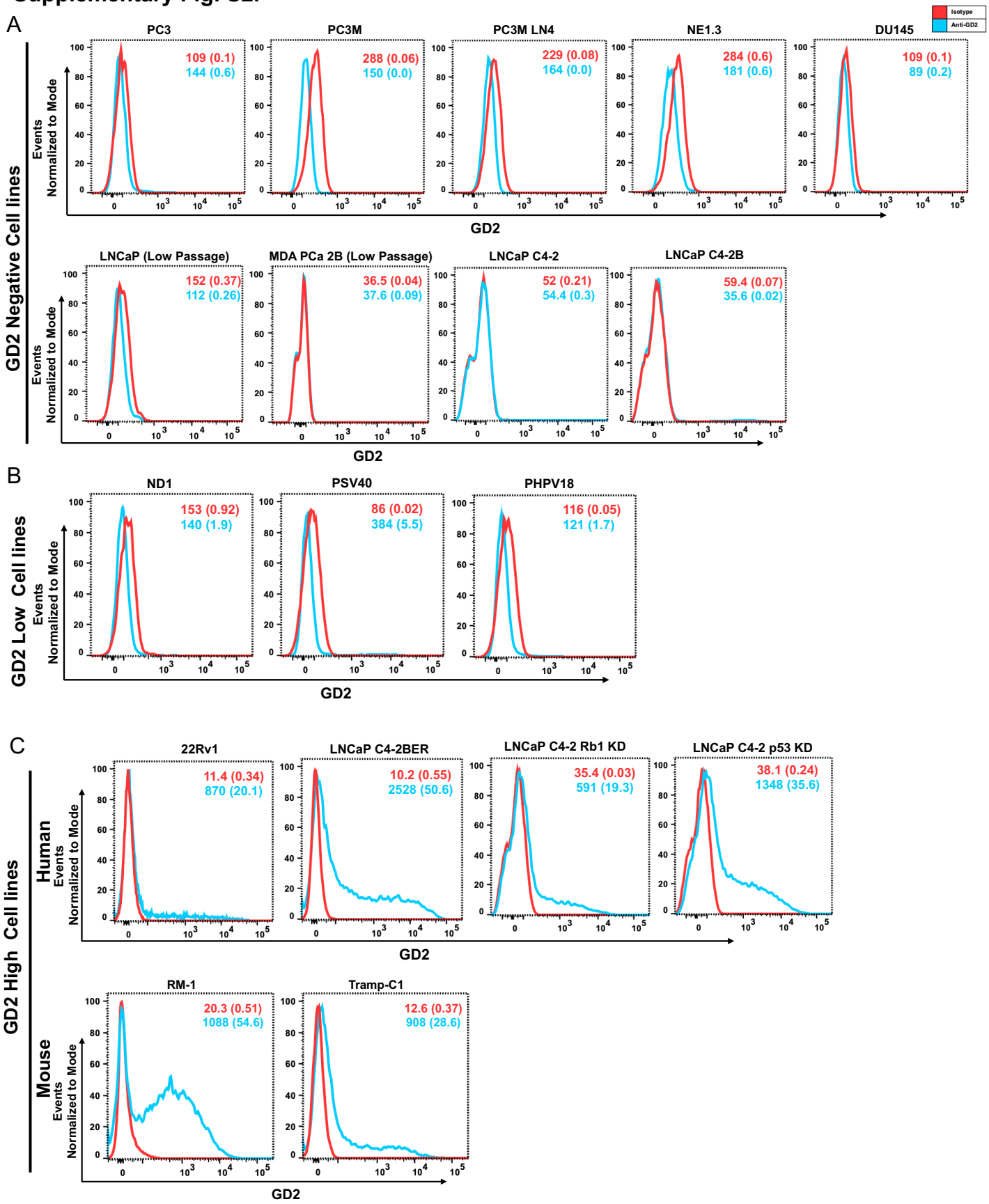

Supplementary Fig. S3.

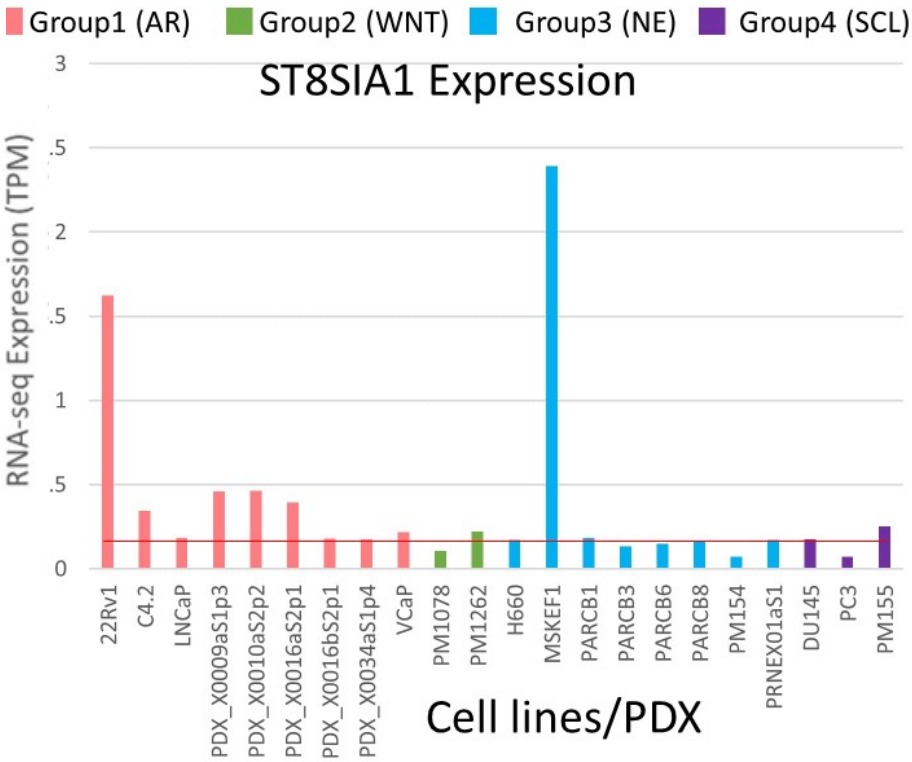

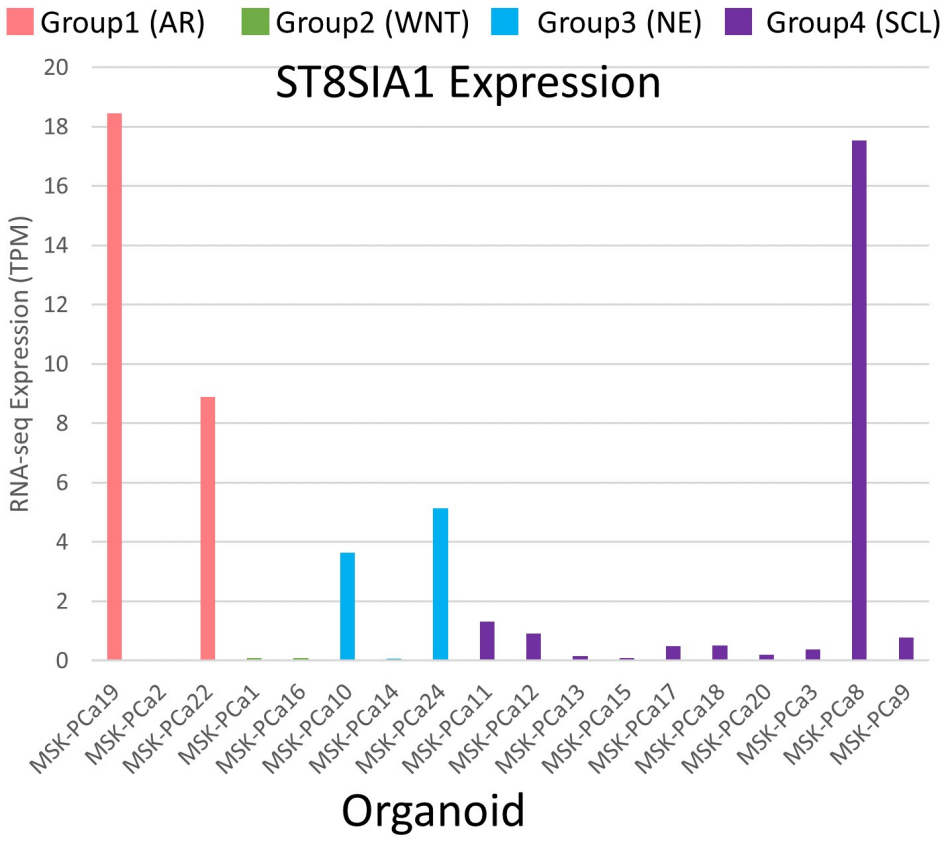

Supplementary Fig. S4

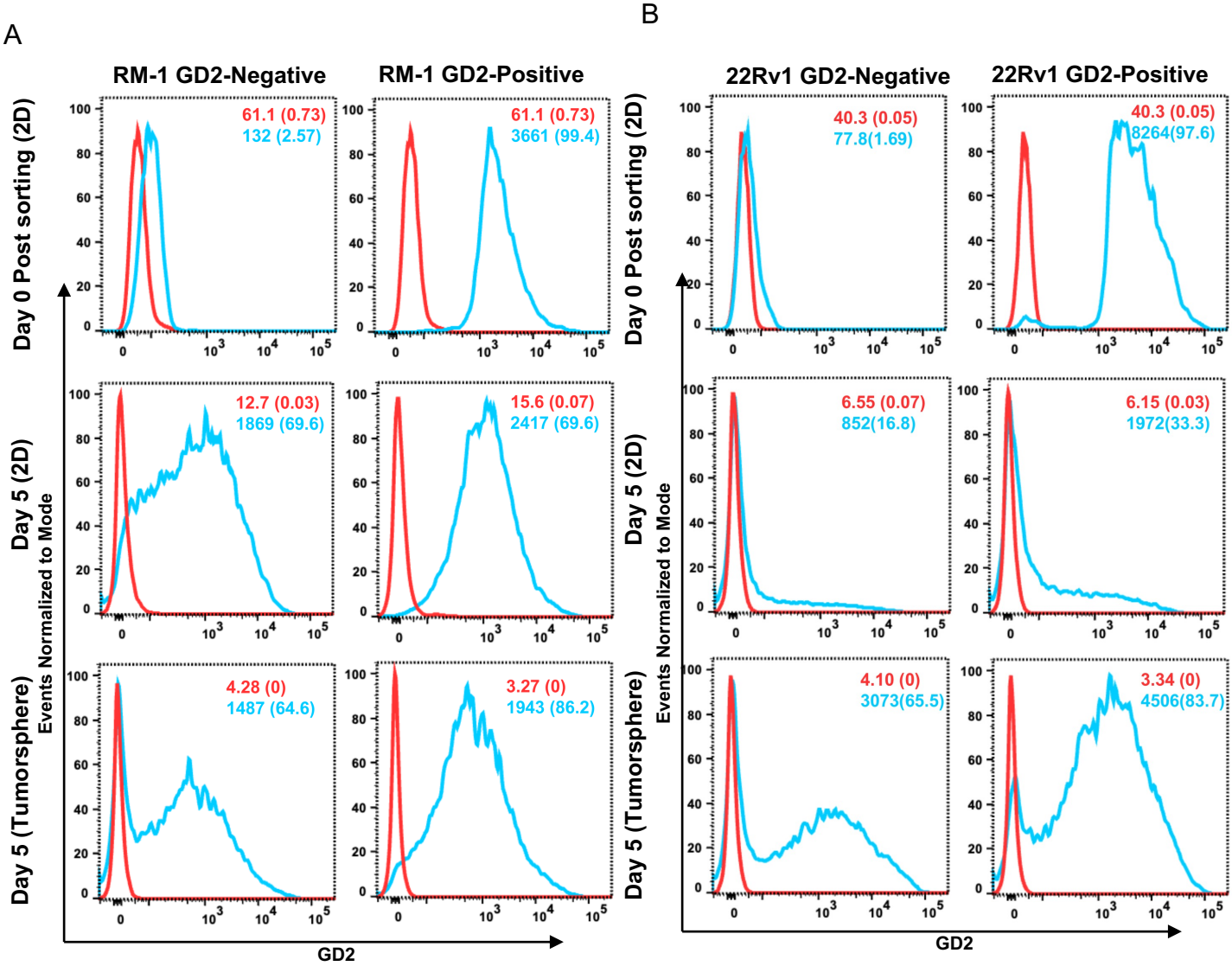
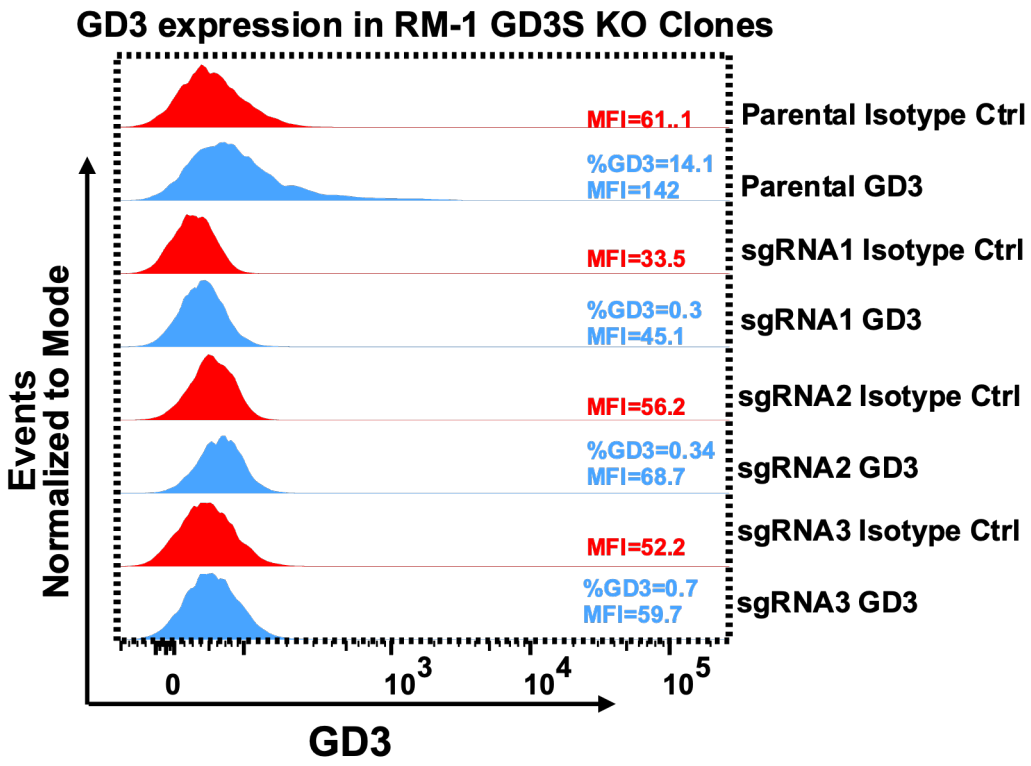
Supplementary Fig. S5